CLM-P694

CLM-P694

UKAEA

Preprint

REVIEW OF SOLAR OBSERVATIONS OF THE n = 2 - 2 TRANSITIONS IN FOURTH PERIOD ELEMENTS

K. D. LAWSON
N. J. PEACOCK

CULHAM LABORATORY
Abingdon Oxfordshire

1983

CLM-P 694

REVIEW OF SOLAR OBSERVATIONS OF THE n = 2 - 2 TRANSITIONS IN FOURTH PERIOD ELEMENTS

K D Lawson* and N J Peacock

Culham Laboratory (Euratom/UKAEA Fusion Association)
Abingdon, Oxon, OX14 3DB, UK

ABSTRACT

A review is made of the solar observations identified with the n = 2 - 2 transitions of elements in the fourth period of the periodic table. The identifications are mainly with transitions of the solar abundant elements calcium and iron. The majority of observations are of solar flares. Some new identifications are presented with transitions belonging to the $2s^2\ 2p^k$ - $2s\ 2p^{k+1}$ transition arrays and within the $2s^2\ 2p^k$ ground configurations.

The transitions are useful for diagnostic purposes, such as the determination of differential emission measures and electron densities of solar flare plasmas. In such applications, it is crucial to know the extent of spectral line blending. Special attention is given to this problem.

Submitted to Astronomy and Astrophysics

*Present address: Department of Applied Physics, University of Hull, Hull, HU6 7RX, England.

November, 1982

1 INTRODUCTION

Emission lines identified with transitions within the $2s^n2p^k$ - $2s^{n-1}2p^{k+1}$ array of the solar abundant elements in the fourth period of the periodic table are observed in the XUV region of active sun and solar flare spectra. There is interest in these transitions because of their use for diagnostic purposes, such as determining differential emission measures [Dere and Cook, 1979] and electron densities [Dere et al, 1979] of the high temperature emitting plasmas. The intense iron lines of this type fall in a window of the quiet sun spectrum and are, therefore, particularly useful for such measurements.

The magnetic dipole transitions within the $2s^n\ 2p^k$ ground configurations occur at longer wavelengths than the $2s^n\ 2p^k$ - $2s^{n-1}2p^{k+1}$ transitions and can be seen throughout the UV spectral region. These transitions are of the same type as the forbidden coronal lines first identified in the visible spectral region by Edlén(1945). In addition to the diagnostic uses referenced above, the longer wavelength magnetic dipole transitions fall in spectral regions which are ideal for the use of high resolution spectroscopy. This allows the measurement of line profiles. From the Doppler broadening or the Doppler shifted components of the lines, information can be obtained about ion temperatures and the mass motions of particular regions within the flare plasma [Cheng et al, 1979]. It should be noted that, in cases where the broadening is extreme, similar information can be obtained from the shorter wavelength resonance lines [Widing and Spicer, 1980].

An analysis of laboratory spectra of the elements in the periodic table from chromium to nickel [Lawson and Peacock, 1980], together with other results reviewed by Fawcett (1975), has led to a complete determination of the term schemes of the $2s^n2p^k$ configurations in the solar abundant elements in the fourth period of the periodic table. Because of the usefulness of the n = 2 - 2 transitions in diagnostic applications, it seems appropriate to review the solar observations of these transitions made to date.

All relevant solar observations known to the authors have been studied in compiling the listings. Those used are mainly observations of solar flares, although some of the transitions occur in the active sun. More details of the experimental conditions under which the observations were made are given in the next section.

In this study, it became evident that a significant number of observed lines were blends, particularly in the region to shorter wavelengths than 400 Å. Clearly, a knowledge of the blending of lines is essential if the line intensities or profiles are to be used in a diagnostic application. Special attention is given to this problem, any evidence or possibility of blending being noted.

The application of the identifications reviewed in this study to the measurement of electron densities in solar flare plasmas is the subject of a subsequent paper [Lawson and Peacock, 1983].

2 SOLAR OBSERVATIONS

A number of authors report XUV spectra of the quiet and active sun; only the more recent of these are of interest in the present study. Of the spectra recorded photoelectrically, Manson (1972) compares the intensities of spectra of a very quiet and of an active sun. These are the results of rocket flights on 3 November 1965 and 8th August 1967, respectively. Malinovsky and Heroux (1973) report observations made from a rocket flown on 4 April 1969. At this time, there was some solar activity, but no flares occurred during the flight. Measurements of the intensities of classified lines due to radiation from the whole solar disc are presented.

In an analysis by Widing and Sandlin (1968), Manson's observations of the very quiet sun, initially reported by Manson (1967, 1968), are used in conjunction with photographically recorded spectra to give classifications and intensities of lines falling in the wavelength range 33 -110 Å. Freeman and Jones (1970) present the results of three rocket flights, launched on 20 March 1968, 17 April 1969 and 20 November 1969. The spectra were recorded photographically, the absolute intensity calibration of the film being determined.

The high resolution possible with photographic records has been exploited by Behring et al (1972, 1976). These authors present listings of wavelengths that are the most accurate available for the XUV spectral region. In addition, many new identifications are given. The spectra used in their analyses were observed from rockets flown on 16 May 1969 and 21 September 1973. A further experiment in which photographic spectra were obtained is described by Firth et al (1974), who give the results of a rocket flight on 14 March 1973. Three spectrographs were used, two observing the quiet solar disc and the third a region above the solar limb.

The only observations of solar flare spectra below a wavelength of 170 Å are those of Kastner et al (1974). The spectra were recorded photoelectrically from the Orbiting Solar Observatory (OSO)-5 satellite in 1969. The intensities of the observed lines were found to be extremely variable, both from flare to flare and throughout the lifetime of a single event. Out of the many flares observed, the spectra of five flares have been studied in detail, special attention being given to the strongest two. Kastner et al identified some of the spectra with $2s^22p^k - 2s2p^{k+1}$ transitions in iron. These identifications have been modified and extended by Fawcett and Cowan (1975), Feldman (1976) and Kononov et al (1976a).

The majority of XUV solar flare observations to longer wavelengths than 170 Å were made using the NRL spectroheliograph in the Apollo Telescope Mount (ATM) on Skylab. Two important exceptions are the results given by Neupert (1971) and Purcell and Widing (1972). These are among the first observations of high temperature lines in this wavelength region. Neupert reports an identification of the lithium - like doublet in iron, observed in spectra from OSO-3. Purcell and Widing present various identifications of images in rocket spectroheliograms with argon, calcium and iron transitions. The rocket was launched on 4 November 1969.

The Apollo Telescope Mount on Skylab carries two NRL spectrographs. The one denoted by S082A is an objective grating spectroheliograph, which photographs dispersed images of the sun between 170 and 630 Å with a spatial resolution of about 3". In spectra recorded with this

instrument, Widing (1975) and Widing and Purcell(1976) have identified and determined improved wavelengths of beryllium- and lithium-like transitions in various elements. Dere (1978) has compiled an almost complete list of lines measured on flare plates recorded with the spectroheliograph. The high temperature lines are classified according to the temperature of the emitting plasma by Sandlin et al (1976) and Widing (1978). These authors, also, make a number of identifications, the latter with forbidden transitions within the $2s^2 2p^k$ ground configurations.

A spectral region not covered by either NRL/ATM instrument is that from 630 to 970 Å. One n = 2 - 2 transition occurring in this region, which is expected to have sufficient intensity to be observed in solar flares is the forbidden transition within the ground configuration of boron-like iron. An observation of this transition from the OSO-6 satellite is reported by Noyes (1972). The theoretical data enabling this identification to be made was provided by Kastner (1971).

The XUV spectra originate in either solar flares or the solar corona. To longer wavelengths, the spectra also contain features which originate in the cooler chromosphere - corona transition zone and the chromosphere. Features from the latter region dominate the spectrum as the visible region is approached. Consequently, there are proportionally fewer high temperature lines as one progresses through the VUV and visible regions of the spectrum. In addition, high temperature lines expected to be present are, sometimes, masked by the spectrum originating in the cooler solar regions. Despite the VUV and visible regions being comparatively unrewarding in a study of high temperature lines, the information which can be readily gained from measurements of the profiles and shifts justifies a search of the available spectra for the few observations of n = 2-2 transitions which might be seen.

One of the latest rocket flights in which spectra of the VUV region were photographed is reported by Ridgeley and Burton (1972). The flight was on 5 August 1971. Solar limb and disc spectra were recorded in the wavelength range 550 to 2000 Å with the aim of studying the structure of the transition zone.

The NRL/ATM instrument on Skylab used for observing the wavelength region 970 to 4000 Å is a double dispersion, normal incidence grating spectrograph, denoted S082B. Flare observations of three forbidden lines of highly ionised iron made with this instrument are reported by Doschek et al (1975). Sandlin et al (1977) and Sandlin and Tousey (1979) give more accurate wavelength measurements of these lines, together with a listing of coronal and transition zone lines. The lines are classified according to the temperature of the emitting plasma. Cheng et al (1979), also, give an improved wavelength for the Fe XX, forbidden line at 1354Å. A complete list of the spectral lines in this wavelength region emitted by the solar flare on 15th June 1973 is reported by Cohen et al (1978).

Results from the Harvard ultraviolet instrument in the Apollo Telescope Mount on Skylab, a near-normal incidence spectrometer-spectroheliometer, are presented by Vernazza and Reeves (1978). Intensities of a composite or averaged spectrum in the wavelength range 280 to 1350 Å are given for different solar structures. The use of a photoelectric detecting system limited the spectral resolution to about 1.6 Å (FWHM). With this resolution, it is expected that a very significant number of the observed lines will be blends, particularly at the shorter wavelengths.

Another group who have made VUV observations of the flaring and non-flaring sun is that at the Crimean Astrophysical Observatory. Bruns et al (1979) report results obtained with the Orbiting Solar Telescope - 1 on board Salyut-4. Like the NRL/ATM, S082B instrument, their spectrograph employs two gratings orientated so as to give dispersion in directions at right angles to each other. In this case, however, each grating is used in a Wadsworth mount, this resulting in spectra having low astigmatism. None of the spectral lines Bruns et al report appear to originate in the very high temperature plasmas found only in flares. Their tentative identification of the line at a wavelength of 1354.3Å as being a blend of CI and FeXXI is thought incorrect, given the absence of any other high temperature lines; this line would appear to be correctly identified with the CI transition.

Several publications concerning observations in the visible region of the spectrum are of interest in the present study. Dollfus (1957) presents the results of an analysis, giving classifications determined from the spatial distributions of line intensities. These classifications are in agreement with those according to ionisation potentials, which, together with the majority of identifications, were given by Edlén (1942). The spectra were obtained, chiefly by Lyot, using a coronograph in 1936 to 1938 (Lyot 1939) and during the eclipse in 1952 (Lyot and Dollfus 1953). Waldmeier (1951) and Pecker et al (1954), also, present observations of high temperature lines which provide further confirmation of Edlén's identifications. More recently, Jefferies et al (1971) reports observations made during the eclipse in 1965.

3 REVIEW OF SPECTRAL CLASSIFICATIONS

A study of the XUV spectra of the elements in the periodic table from chromium to nickel has enabled the term schemes of the $2s^n\ 2p^k$ configurations of these elements to be almost completely determined (Lawson and Peacock 1980). Together with other results, reviewed by Fawcett (1975), these data enable the term schemes of the $2s^n\ 2p^k$ configurations to be found for the solar abundant elements in the fourth period of the periodic table.

Also used in the present study are the semi-empirical extrapolations of Edlen (1979a,b, 1981a,b, 1982). These extrapolations enable the experimental data to be smoothed, resulting in more accurate wavelengths and providing a check on previous identifications. This has allowed an apparent inconsistency in the boron-like sequence to be explained; the details are discussed in the appropriate section below.

In cases where there are neither direct observations from which to construct the term scheme, nor semi-empirical extrapolations, wavelengths have been derived from graphical extrapolations in which the first differences of the wavenumbers have been plotted against the atomic number.

Theoretical relative line intensities for chromium, iron and nickel appropriate to the electron densities expected in the solar corona and solar flares, typically 10^{10} to $10^{12}cm^{-3}$, were obtained from the references listed in Lawson et al (1981). Estimates of the line intensities for calcium were made by extrapolating these data and those given by Bhatia et al (1980) for titanium.

In compiling the listings of classifications, all appropriate observations known to the authors have been considered. The most important experiments have been described in section 2, although not all of those described have results identified with the n = 2-2 transitions of interest. Where identifications have been given in the references, they have been checked against the present list of wavelengths and intensities. A search was then made to see if any further identifications could be made.

Tables 2 to 8 list the solar observations identified with n = 2-2 transitions of fourth period elements. Tentative identifications are discussed in the appropriate section of the text. In addition to the solar wavelengths, calculated or laboratory wavelengths of each transition are given for comparison. These are mainly from the semi-empirical calculations of Edlén. Since the solar line intensities and temperature or enhancement classifications are important in making the identifications, these are included in the tables. More details about the various classification schemes used by the different authors are presented in table 9. This table also explains the intensity scales and the meaning of the other notations used.

In any diagnostic application, it is essential to know the extent of spectral line blending. Consequently, an important aspect of this study was to check any possibility of line blending. In some cases, the solar observation is described as being a blend of lines in the original reference. In others, it has become evident that certain lines must be blends. Anomalously high intensities, wavelength discrepancies between solar and calculated values and wavelength coincidences of transitions, both expected to have observable intensities normally indicate blends. In addition, lists of quiet and active sun lines have been checked to see if there is any likelihood of blends between previously observed lower temperature lines and the reviewed lines. In this check, only the first order of the quiet and active sun spectra were considered. Where there is any evidence of blending, this is noted in the final column of tables 2 to 8.

The inclusion of coincident quiet and active sun lines in the tables, even when there is no definite evidence of blending, is thought important, because the lower temperature lines can be greatly enhanced in solar flares. For example, the $2s^2\ 2p^k - 2s2p^{k+1}$ transitions of iron appear in a window of the quiet sun spectrum between wavelengths of 90 and 145Å. This is well illustrated in spectra presented by Kastner et al (1974). Therefore, it might be expected that these lines would be free from blending. However, with the spectral resolution possible in the photoelectric system used by Kastner et al, this is not the case. There is significant blending both between the n = 2 - 2 transitions and with enhanced quiet and active sun lines, particularly for the transitions in the CI isoelectronic sequence.

Of the experiments listed in table 1, those of most interest are the OSO-5 solar flare observations reported by Kastner et al (1974) and the NRL/ATM spectroheliograph observations. The latter are presented by a number of authors. It should be noted that there appears to be a systematic wavelength error in the results of Kastner et al between wavelengths of 110 and 120Å. This is illustrated in figure 1, in which the difference between the solar and calculated wavelengths of identified lines are plotted against the calculated wavelengths.

FI Isoelectronic Sequence

The solar observations identified with transitions in the FI isoelectronic sequence are listed in table 2. It can be seen that the fluorine-like doublet of iron is observed in active sun spectra.

In all but one case, it would appear that the iron doublet lines are blended. The exception is the observation by Behring et al (1972, A) of the $2s^22p^5\ {}^2P_{3/2} - 2s2p^6\ {}^2S_{1/2}$ transition at 93.933Å; in this case, the Fe X line at 94.012Å is seen as a separate line. Behring et al describe the other member of the doublet, the ${}^2P_{1/2} - {}^2S_{1/2}$ transition at 103.928Å, as being wide. Since there is no obvious difference between the lines in well

resolved laboratory spectra, it is thought that this indicates blending with the unidentified quiet sun line, whose wavelength, given by Manson (1972), is 103.89Å.

In addition to being blended with the FeX transition, the line reported by Kastner et al (1974, K) at 93.94Å is thought to be blended with the Fe XX, $2s^22p^3\,^2D_{5/2}$ - $2s2p^4\,^2P_{3/2}$ transition at 93.79Å. The additional line component at 94.1Å noted by Kastner et al is probably due to the Fe X transition.

The calculated wavelengths for the allowed transitions in this sequence are taken from Edlén (1981a). Wavelengths for the forbidden transition are the results of an extrapolation by Stamp (1983). This extrapolation includes recent tokamak measurements and is thought to be an improvement on previous extrapolations.

OI Isoelectronic Sequence

The classifications of lines with oxygen-like transitions are given in table 3. No allowed transitions in calcium or nickel have been observed in this sequence. Of the identifications with forbidden transitions, one is tentative. This is the line reported by Cohen et al (1978, D) at 1133.68Å, which is identified with the $2s^22p^4$ ($^3P_2$ - $^1D_2$) transition of calcium, the strongest of the transitions within this configuration. This is suggested as an alternative to the tentative identification of this line with the Fe II, $3d^6$ (a^5D) 4s a $^6D_{9/2}$ - $1^0_{7/2}$ transition made by Cohen et al. Without further information, such as a temperature classification, no definite identification cah be made.

The line observed by Kastner et al (1974, K) at 91.21Å, if correctly identified with the $2s^22p^4\ ^1D_2$ - $2s2p^5\ ^1P_1$ transition of iron, must be blended to explain the significant discrepancy of 0.19Å between the observed and calculated wavelengths. The other component of the blend is most likely the Fe XXI, $2s^22p^2\ ^3P_0$ - $2s2p^3\ ^3S_1$ transition. There may also be a component of the quiet/active sun line at 90.96/91.004Å in the line at 91.21Å.

The low type classification of the line at 106.28Å (Kastner et al) is probably explained by blending with the Ne VII, $2s2p^3P_2$ - $2s3d^3D_3$ transition. Other possible blends are noted in table 3.

There is no convincing evidence for the tentative identification made by Vernazza and Reeves (1978) of the solar line at 592.5Å with the $2s^22p^4(^3P_2$ - $^1D_2)$ transition in iron. They suggest that this line is a blend of the Fe XIX transition with a S XI transition. A significant contribution from Fe XIX would be expected to result in a much greater enhancement of the intensity of the active sun line over that of the quiet sun line than is seen. This is only a factor of 4 to 5. Lower ionisation stages of sulphur

show similar or greater enhancements. This identification has, therefore, been omitted from table 3. It should be noted that the reported observations of the $2s^22p^4$ ($^3P_2$ - $^1D_2$) transition in iron are not expected to be blended with the S XI transition; they were observed with the NRL/ATM spectroheliograph, an instrument with a much higher resolution than the Harvard/ATM spectrometer.

The calculated wavelengths listed for this sequence are from Edlen (1981a, 1982), the latter reference being used for the forbidden transitions.

NI Isoelectronic Sequence

The NI isoelectronic sequence is the highest in which calcium lines are positively identified in the XUV region of active sun spectra. This is somewhat unexpected; the temperature of the maximum abundance of Fe XVIII ions under ionisation equilibrium, the highest ionisation stage of iron observed in active sun spectra, corresponds to that of beryllium- or lithium-like calcium (Jordan 1969, 1970).

The $2s^22p^3\ ^2D_{5/2}$ - $2s2p^4\ ^2P_{3/2}$ transition of Fe XX is thought to be present in the spectra of Kastner et al (1974, K). At all likely electron densities, it is expected to be more intense than the observed $2s^22p^3\ ^2D_{3/2}$ - $2s2p^4\ ^2D_{3/2}$ transition. However, it will be masked by the strong $2s^2\ 2p^5\ ^2P_{3/2}$ - $2s2p^6\ ^2S_{1/2}$ transition of Fe XVIII, this explaining the significant wavelength discrepancy.

The lines reported by Kastner et al at wavelengths of 113.45, 118.70 and 121.85Å are expected to be due mainly to Fe XX transitions, although they may contain components of other transitions. These transitions are noted in table 4, which lists the classifications for the NI sequence. In contrast, the line at 132.83Å is chiefly due to the very intense beryllium-like $2s^2\ ^1S_0$ - $2s2p\ ^1P_1$ transition of iron.

The line listed by Widing (1978) at 478.08Å was identified with the $2s^22p^3$ ($^4S_{3/2}$ - $^2D_{5/2}$) transition in nickel (Lawson et al, 1981). The semi-empirical extrapolations of Edlén (1982) give a calculated wavelength for this transition of 477.7Å, showing that this identification is incorrect.

The calculated wavelengths for the forbidden transitions in table 4 are, also, taken from Edlén (1982). To date, no semi-empirical extrapolations are available for the allowed transitions in this sequence and the wavelengths of laboratory observations are given. For the transitions in calcium, these are taken from Kononov et al (1976b) and for iron from Lawson et al (1981).

CI Isoelectronic Sequence

The most notable aspect of the observations of the n = 2-2 transitions in the CI isoelectronic sequence, listed in table 5, is the large number that are blended. In addition, observed solar lines coincide with several of the remaining CI lines, although in these cases, there is no direct evidence of blending.

In the $2s^22p^2$ - $2s2p^3$ transition array of Ca XV, the $^3P_1$ - $^3P_1$ transition is expected to have an observable intensity, but is blended with an unidentified line at 176.982Å. The $^3P_1$ - $^3P_0$ transition is weaker, so may not be present; in any case, it is blended with an Fe X transition. Dere (1978, E) identifies the solar line at 208.33Å as a blend between the $^3P_1$-$^3D_1$ transition and a SX transition. A component of the $^3P_1$ - $^3D_1$ transition of Ca XV may well be present in this line and would be favoured by low electron densities. Nevertheless, it is expected to be weak and the line is thought to be due mainly to SX.

The identification of the $2s^22p^2\ ^3P_{1/2}$ - $2s2p^3\ ^5S_2$ transitions in iron by Dere (1978, E) led to a search for observations of these transitions in calcium. The wavelength predictions given by Kastner et al (1977) are 391 and 421Å, respectively. Graphical extrapolations using the results of Lawson and Peacock (1980) and the observation of the transitions in neon (Ridgeley and Burton 1972) resulted in somewhat lower predictions of 383.8 and 412.9Å. The Ca XV ions emit high temperature lines and Widing (1978, X) lists lines at 382.82 and 411.61Å, which are given a temperature classification of II, typical ions being Ca XV to Ca XVII. A search of the list reported by Dere (1978) shows that these are the only lines in this spectral region of any temperature classification with the expected wavelength separation. Edlén (1982) calculates a $2s^2\ 2p^2\ (^3P_1 - ^3P_2)$ splitting of 18,360cm^{-1}, whereas the observed splitting is 18,271cm^{-1}. Both lines are blended with lower temperature lines, this, possibly, explaining the discrepancy. These identifications are tentative, but it appears that they are the only possible ones, if both transitions have an observable intensity.

It should be noted that the isoelectronic sequence suggested by Vernazza and Reeves (1978) for the $2s^22p^2\ ^3P_1$ - $2s2p^3\ ^5S_2$ transition cannot be made to fit an extrapolation which includes the observation of the transition in iron (Dere 1978, E). The graphical extrapolation being used in the present study differs markedly from all of the new identifications made by Vernazza and Reeves. Their wavelength for the F IV transition is in agreement with the tentative identification of this transition made by Sandlin et al (1977).

Sandlin et al (1977, T) also, make a tentative identification of the $2s^22p^2$ ($3p_2$ - $^1D_2$) transition of Ca XV with the solar line at 1375.95Å. Given the classification of this line as a high temperature line, it is thought that this identification is correct; the transition is expected to

be one of the most intense within the configuration. However, it should be noted that there is a small wavelength discrepancy with Edlén's (1982) calculated value of 1375.88Å. If the latter wavelength proves correct, it is likely that this line will be blended in many spectra with a Ni II transition at 1375.822Å.

The apparent discrepancies between the theoretical intensities of the Fe XXI transitions (Mason et al 1979) and the observed intensities reported by Kastner et al (1974, K) are explained by line blending. The emission from Fe XXI is found to be comparatively weak in these spectra, this being especially so in the spectrum of flare E whose lines have intensities a factor of 7 weaker than those of flare B. Clearly, the intensities of those lines which are not significantly affected by blending should reflect this difference. There are only four such lines. An added complication is that one of these four is a blend of two Fe XXI transitions, the $2s^22p^2\,{}^3P_1$ - $2s2p^3\,{}^3D_{1,2}$ transitions.

Of the Fe XXI lines which are components of blends, the $2s^22p^2\,{}^3P_2$ - $2s2p^3\,{}^3S_1$ and $2s^22p^2\,{}^3P_1$ - $2s2p^3\,{}^3P_1$ transitions are expected to be present in the spectra of Kastner et al. The latter is blended with the beryllium-like $2s^2\,{}^1S_0$ - $2s2p\,{}^1P_1$ transition of nickel to form the observed line at 117.81Å. However, both of these transitions are expected to give rise to a line with a type IV enhancement classification whereas the line at 117.81Å has a type III classification. Kastner et al note that in flare E this line is observed on the shoulder of a neighbouring line, the intense Fe XXII line at 117.18Å. This gives a possible explanation of the low enhancement classification; it is the same as that for the line at 117.18Å, which contains a component of an active sun line.

The $2s^22p^2\,{}^3P_2$ - $2s2p^3\,{}^3S_1$ transition must be supposed blended with a line near 102.4Å, to explain the significant discrepancy between the solar and laboratory wavelengths, 102.35 and 102.22Å, respectively. No line near 102.4Å has been reported. It should be noted that, even in a spectrum which is more highly resolved, the ${}^3p_2$ - ${}^3S_1$ transition may still be blended, being affected by an active sun line at 102.15Å.

The other blended Fe XXI lines are expected to be weaker and it is not possible to say with certainty whether they are present in the spectra of Kastner et al. Their identifications are, therefore, regarded as being tentative.

The $2s^22p^2\,{}^3P_2$ - $2s2p^3\,{}^3P_1$ transition, if it is present at all in the line at 123.76Å, must be blended. This transition is expected to be weaker

than the unblended $2s^22p^2\,^3P_2$ - $2s2p^3\,^3P_2$ transition at 121.17Å. Consequently, it is necessary to account for the greater intensity of the former, as well as the absence of a change in intensity between the two flares. The nearest observed solar line is at 123.492Å and, therefore, it is necessary to suppose the existence of an unreported line closer to the wavelength of 123.76Å.

The solar line at 97.88Å is reported by Feldman (1976, I); although one of the OSO - 5 results, it is not given in the list of Kastner et al (1974).

As in the NI isoelectronic sequence, no semi-empirical extrapolation for the allowed transitions are available and, therefore, observed wavelengths are given in table 5. Those for calcium are from Kononov et al (1976,b) two wavelengths being adjusted so as to be consistent with the wavelengths of the magnetic dipole transitions. The latter are taken from Edlén (1982). Calculated wavelengths, as discussed above, are given for the Ca XV, $2s^22p^2\,^3P_{1,2}$ - $2s2p^3\,^5S_2$ transitions.

For iron the observed wavelengths are taken from Lawson et al (1981). The wavelengths for the iron triplet-quintet intercombination lines are calculated from the term schemes of Lawson and Peacock (1980). This demonstrates the consistency between the solar and laboratory observations as to the positioning of the $^5S_2$ level. The wavelength of the forbidden $2s^22p^2$ ($^3P_0$ - $^3P_1$) transition in iron comes from Edlén (1982).

BI Isoelectronic Sequence

As in the CI isoelectronic sequence, the listing of identifications with boron-like transitions, table 6, contains a number of blended lines. In contrast, however, the emission from boron-like iron in the spectra of Kastner et al (1974, K) is comparatively intense. This led to a search of these spectra for boron-like calcium and nickel lines.

The most intense $2s^22p$ - $2s2p^2$ transition of calcium is expected to be the $^2P_{3/2}$ - $^2P_{3/2}$ transition and this is identified with the line at 164.14Å in the spectra of Kastner et al. This transition is most likely blended with the Ni XIV transition identified by Behring et al (1972, A; 1976, B) with the line at wavelengths of 164.146 and 164.13Å, respectively. The lines observed by Behring et al may well contain a component of Ca XVI.

The $2s^22p^2P_{3/2}$ - $2s2p^22P_{1/2}$ transition of calcium, although weaker than the $^2P_{3/2}$ - $^2P_{3/2}$ transition, might, also, appear in the spectra of Kastner et al, as a component of the line at 167.50Å. This line is thought mainly due to an Fe VIII transition. However, it should be noted that the other members of the Fe VIII multiplet do not appear in these spectra; in the

absence of other blended components to the 167.50Å line, this would suggest that the $^2P_{3/2}$ - $^2P_{1/2}$ transition intensity is significant.

Within the $2s^22p$ - $2s2p^2$ array of nickel, the transition with the highest theoretical intensity, the $^2P_{1/2}$ - $^2S_{1/2}$ transition, can be identified with the line at 104.60Å reported by Kastner et al.

Given the systematic error in the wavelength calibration of the spectra of Kastner et al, shown in figure 1, the $2s^22p^2P_{3/2}$ - $2s2p^22P_{3/2}$ transition in iron would be expected to have an observed wavelength in these spectra of about 114.49Å. The discrepancy with the reported wavelength of 114.41Å would suggest that the transition is blended. The nearest observed solar line is due to Mg V at a wavelength of 114.036Å. However, the Mg V line would be expected to be resolved as a separate line.

The high enhancement classification for the line at 114.41Å and the reasonable agreement between the theoretical and observed intensities of the allowed transitions in this sequence would suggest that most of the emission in this line is due to Fe XXII. If so, the $2s^22p^2P_{1/2}$ - $2s2p^22P_{3/2}$ transition might appear weakly in the spectra. The nearest line to the calculated wavelength of 100.768Å is that at 100.89Å. To explain the wavelength discrepancy and the low enhancement classification of this line, only type II, it is necessary to suppose that the line is a blend with a longer wavelength line, possibly the unidentified line reported by Manson (1972) at 101.01 and 100.96Å.

The inconsistency between wavelengths of the solar identifications of transitions within the $2s^22p^2P$ - $2s2p^24P$ multiplet in iron made by Sandlin et al (1976) and laboratory measurements of boron-like transitions (Lawson and Peacock 1980) has been explained by Edlén (1981b). Semi-empirical extrapolations have indicated errors in a few of the laboratory wavelengths, which, when corrected, allow both the solar and laboratory wavelengths to be fitted to the same term schemes.

It should be noted, however, that the intensities of the solar observations are still not as expected, even allowing for the blends given in table 6. For example, the $2s^22p^2P_{1/2}$ - $2s2p^24P_{1/2}$ transition is expected to be at least 3 times stronger than the $2s^22p^2P_{3/2}$ - $2s2p^24P_{3/2}$ transition, at solar electron densities. This would suggest the possibility of there being even more blends.

Semi-empirical extrapolations are available for all boron-like levels. The wavelengths of transitions within the $2s^22p$ - $2s2p^2$ transition array are

taken from Edlén (1981b), some of these being adjusted to fit that for the forbidden transition within the ground configuration of iron. The latter is from Edlén (1982).

Be I Isoelectronic Sequence

A striking feature of the classifications of solar lines isoelectronic with Be I is the extreme intensity of the Fe XXIII, $2s^2\,^1S_0$ - $2s2p\,^1P_1$ transition observed in one of the spectra reported by Kastner et al (1974, K) at 132.83Å. Although blended with the Fe XX, $2s^22p^3\,^4S_{3/2}$ - $2s2p^4\,^4P_{5/2}$ transition, most of the emission is due to Fe XXIII. Kastner et al note that the line is more intense than the Fe IX, quiet sun line at 171.08Å, which is emitted from the whole disc of the sun.

The identification of Vernazza and Reeves (1978, U) of a line at 371.4Å with the $2s^2\,^1S_0$ - $2s2p\,^3P_1$ transition of Ca XVII is thought questionable. Certainly, if this transition was a significant component of the line a much greater enhancement of the intensity would be expected in the active sun spectrum. Nevertheless, the temperature of active solar regions appears to be sufficient for this ionisation stage to be present and, consequently, the transition might contribute some emission to the line.

The identification of the $2s^2\,^1S_0$ - $2s2p\,^1P_1$ transition of Mn XXII must be regarded as being tentative. It is the only observation of manganese in the spectra of Kastner et al (1974, K) and there is a small wavelength discrepancy, not explained by blending with the Ca XII, $2s^22p^5\,^2P_{3/2}$ - $2s2p^6\,^2S_{1/2}$ transition. As confirmation, it would be desirable to make an identification of the corresponding transition in the marginally more abundant chromium. However, the chromium transition, which occurs at a wavelength of 149.89Å, will be masked by the intense OVI, $2s\,^2S_{1/2}$ - $2p\ ^2P_{3/2,1/2}$ transitions at 150.05Å.

It should be noted that the line at 117.81Å identified as a blend of the $2s^2\,^1S_0$ - $2s2p\,^1P_1$ transition in nickel and the $2s^22p^2\,^3P_1$ - $2s2p^3\,^3P_1$ transition in iron, is reported by Kastner et al to be observed on the shoulder of the intense line at 117.18Å. This might explain the low enhancement classification given for the 117.81Å line; both identified components are expected to have the highest classification.

Feldman (1976) identifies the 117.81Å line with the Ni XXII, $2s^22p^3\,^4S_{3/2}$ - $2s2p^4\,^4P_{5/2}$ transition. However, this transition is expected to be much weaker than the nickel, $2s^2\,^1S_0$ - $2s2p\,^1P_1$ transition and,

consequently, only the latter is given in the tables.

The calculated wavelengths for this sequence are taken from Edlén (1981a).

Li I Isoelectronic Sequence

As can be seen in table 8, the lithium-like doublet is observed in several fourth period elements, one member even being identified in titanium. The line at 165.42Å, listed by Kastner et al (1974, K) is identified with the Ni XXVI, $2s^2S_{1/2} - 2p^2P_{3/2}$ transition. Its low enhancement classification and the discrepancy with the calculated wavelength, 165.378Å, can be explained by blending with an Ar X transition.

Semi-empirical extrapolations (Edlén 1974a, b) are used to give the calculated wavelengths.

4 CONCLUSION

A comprehensive review is given of solar observations identified with the n = 2-2 transitions of elements in the fourth period of the periodic table. These transitions occur in the high temperature plasmas found in solar flares and active solar regions.

The spectra are of particular interest because of their uses for diagnostic applications. An understanding of the blending of spectral features is, therefore, crucial. Wherever there is any evidence of blending, this is noted in the review. An example of a diagnostic application is presented in a subsequent paper; electron densities are calculated from line intensity ratios of the solar observations listed in the present study.

It is hoped that the review will form a useful basis from which future identifications can be made, facilitating diagnostic measurements and encouraging future observations of the XUV region of solar flare spectra. It is evident from the study that the most useful observations in the XUV spectral region, particularly at the shorter wavelengths, are those having the highest spectral resolution. This conclusion favours the photographic recording of these spectra.

ACKNOWLEDGEMENTS

We would like to thank H E Mason for useful advice in the early stages of the preparation of this paper.

REFERENCES

Behring W E, Cohen L and Feldman U, 1972, Astrophys J, 175, pp 493-523.
Behring W E, Cohen L, Feldman U and Doschek G A, 1976, Astrophys J, 203, pp 521-7.
Bhatia A K, Feldman U and Doschek G A, 1980, J Appl Phys, 51, pp 1464-80.
Bruns A V, Grechko G M, Gubarev A A, Klimuk P I, Sevast'Yanov V I, Severnyi A B, Steshenko N V and Feoktistov K P, 1979, Bull Crimean Astrophys Obs 59, pp 1-21.
Cheng C C, Feldman U and Doschek G A, 1979, Astrophys J, 233, pp 736-40.
Cohen L, Feldman U and Doschek G A, 1978, Astrophys J Suppl, 37, pp 393-405.
Dere K P, 1978, Astrophys J, 221, pp 1062-7.
Dere K P and Cook J W, 1979, Astrophys J, 229, pp 772-87.
Dere K P, Mason H E, Widing K G and Bhatia A K, 1979, Astrophys J Suppl, 40, pp 341-64.
Dollfus A, 1957, C R Acad Sci Paris, 245, pp 2011-2 (In French).
Doschek G A, Feldman U, Dere K P, Sandlin G D, Vanhoosier M E, Brueckner G E, Purcell J D and Tousey R, 1975, Astrophys J, 196, pp L83-6.
Edlén B, 1942, Zs f Astrophys, 22, pp 30-64 (In German)
Edlén B, 1945, Mon Not R astr Soc, 105, pp 323-33
Eldén B, 1979a, Phys Scr, 19, pp 255-66
Edlén B, 1979b, Phys Scr, 20, pp 129-37
Edlén B, 1981a, Phys Scr, 22, pp 593-602
Edlén B, 1981b, Phys Scr, 23, pp 1079-86
Edlén B, 1982, Phys Scr, 26, pp 71-83
Fawcett B C, 1975, Atom Data Nucl Data Tables, 16, pp 135-64
Fawcett B C and Cowan R D, 1975, Mon Not R astr Soc, 171, pp1-8
Feldman U, 1976, Astrophys Space Sci, 41, pp 155-81
Firth J G, Freeman F F, Gabriel A H, Jones B B, Jordan C, Negus C R, Shenton D B and Turner R F, 1974, Mon Not R astr Soc, 166, 543-60
Freeman F F and Jones B B, 1970, Solar Phys 15, pp 288-308
Jefferies J T, Orrall F Q and Zirker J B, 1971, Solar Phys, 16, pp 103-10
Jordan C, 1969, Mon Not R astr Soc, 142, pp 501-21
Jordan C, 1970, Mon Not R astr Soc, 148, pp 17-23
Kastner S O, 1971, J Opt Soc Am, 61, pp 335-46
Kastner S O, Bhatia A K and Cohen L, 1977, Phys Scr, 15, pp 259-67
Kastner S O, Neupert W M and Swartz M, 1974, Astrophys J, 191, pp 261-70
Kononov E Ya, Koshelev K N, Podobedova L I, Chekalin S V and Churilov S S, 1976a, J Phys B, 9, pp 565-72
Kononov E Ya, Koshelev K N, Podobedova L I and Churilov S S, 1976b, Opt Spectrosc, 40, pp 121-3.
Lawson K D and Peacock N J, 1980, J Phys B, 13, pp 3313-34
Lawson K D and Peacock N J, 1983, Submitted to Astron Astrophys
Lawson K D, Peacock N J and Stamp M F, 1981, J Phys B, 14, pp 1929-52
Lyot B, 1939, Mon Not R astr Soc, 99, pp 580-94
Lyot B and Dollfus A, 1953, C R Acad Sci Paris, 237, pp 855-9 (In French)
Malinovsky M and Heroux L, 1973, Astrophys J, 181, pp 1009-30
Manson J E, 1967, Astrophys J, 147, pp 703-10

Manson J E, 1968, Astrophys J, 153, pp L191-3
Manson J E, 1972, Solar Phys, 27, pp 107-29
Mason H E, Doschek G A, Feldman U and Bhatia A K, 1979, Astron Astrophys, 73, pp 74-81
Neupert W M, 1971, Phil Trans Roy Soc Lond A, 270, pp 143-55
Noyes R W, 1972, Proc Symp on High Energy Phenomena on the Sun, ed R Ramaty and R G Stone, NASA SP-342, pp 231-41
Pecker C, Billings D E and Roberts W O, 1954, Astrophys J, 120, pp 509-20
Purcell J D and Widing K G, 1972, Astrophys, J 176, pp 239-47
Ridgeley A and Burton W M, 1972, Solar Phys, 27, pp 280-5
Sandlin G D, Brueckner G E, Scherrer V E and Tousey R, 1976, Astrophys J, 205, pp L47-50
Sandlin G D, Brueckner G E and Tousey R, 1977, Astrophys J, 214, pp 898-904
Sandlin G D and Tousey R, 1979, Astrophys J, 227, pp L107-9
Stamp M F, 1983, DPhil Thesis, University of Oxford
Vernazza J E and Reeves E M, 1978, Astrophys J Suppl, 37, pp 485-513
Waldmeier M, 1951, Zs f Astrophys, 29, pp 29-32 (In German)
Widing K G, 1975, Astrophys J, 197, pp L33-5
Widing K G, 1978, Astrophys J, 222, pp 735-9
Widing K G and Purcell J D, 1976, Astrophys J, 204, L 151-3
Widing K G and Sandlin G D, 1968, Astrophys J, 152, 545-56
Widing K G and Spicer D S, 1980, Astrophys J, 242, pp 1243-56

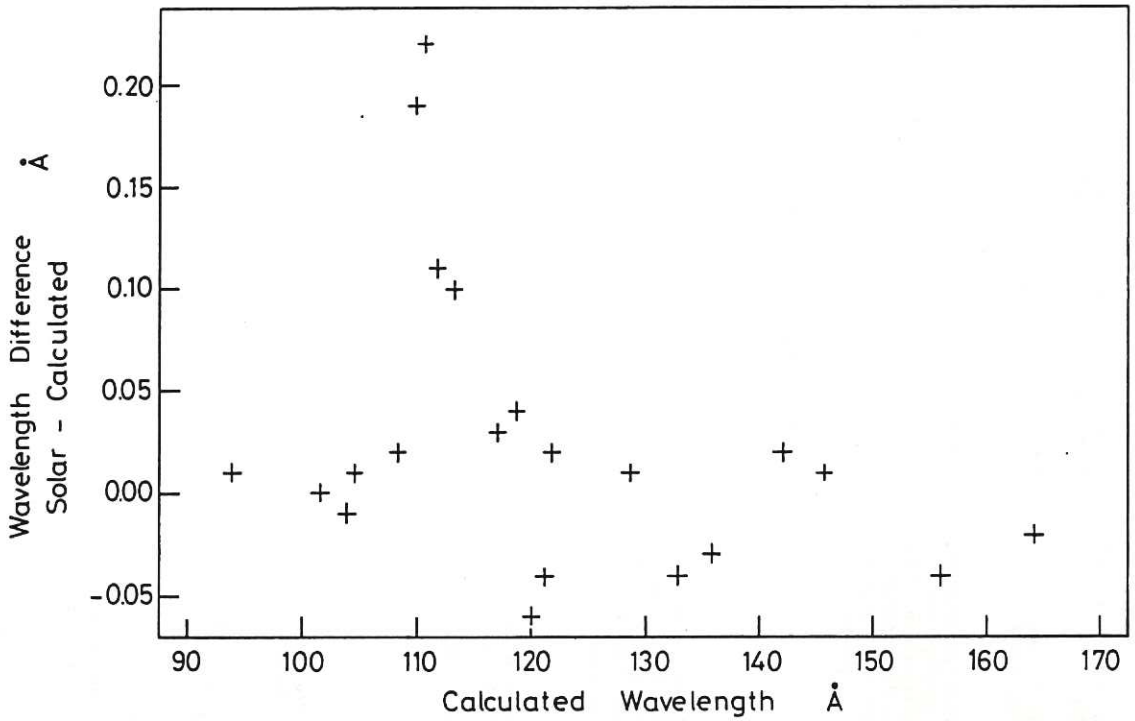

Fig.1 Systematic error in the wavelength calibration of the spectra of Kastner et al (1974).

TABLE 1 Flight data and instrumentation

Reference	Dates of Observations	Observed Solar Feature	Wavelength Range	Spectroscopic Instrument	Location of Instrument	Summary of Results
A Behring et al (1972)	16 May 1969	Moderately active disc	60 - 385Å	Concave grating spectrograph, g. r = 3m, i = 88°, 1200 lines mm^{-1}. Spec res, 0.04Å.	Aerobee 150 rocket from WSMR	High resolution spectra giving most accurate wavelengths available, with identifications.
B Behring et al (1976)	21 September 1973	Quiet disc	160 - 770Å	Concave grating spectrograph, g. r = 3m, i = 88˘, 600 lines mm^{-1}. Spec res, 0.06Å.	Aerobee 200 rocket from WSMR	Composite high resolution spectra, including results from A, giving most accurate wavelengths available, with identifications.
C Cheng et al (1979)	15 July 1973 to 9 September 1973	Flares	1354Å	Double-dispersion, concave grating spectrograph, S082B, n. Dispersions crossed; predisperser grating ruled so as to reduce astigmatism. Main grating :r = 2m, 600 lines mm^{-1}. Predisperser grating: r = 0.5m, 300 lines mm^{-1} for 970-1970Å, 150 lines mm^{-1} for 1940 - 3940Å. Spec res, 1 in 30,000. Spat res, 2" x 60".	Skylab NRL/ATM	Measurement of line widths of Fe XXI, 1354 forbidden line, with comparison of ion temperatures with ionisation equilibrium calculations.
D Cohen et al (1978)	15 June 1973	Flare	977 - 1940Å	S082B spectrograph	Skylab NRL/ATM	List of spectral lines for 15 June 1973 flare, with identifications and absolute line intensities.
E Dere (1978)	May 1973 to February 1974	Flares	171 - 630Å	Slitless, concave grating spectroheliograph, S082A, employing Wadsworth mount, n. Grating rotated to select ranges 175-335Å and 320-480Å. r = 4m, 3600 lines mm^{-1}. Spec res, highest observed, 0.1Å. Spat res, 3" for above wavelengths.	Skylab NRL/ATM	Almost complete list of XUV flare lines, with identifications.
F Dollfus (1957)	1936 - 1938; 25 February 1952	Corona; corona during eclipse	3350-8300Å; visible, near ultraviolet	1936-8: Coronograph equipped with plane grating spectrograph, employing Littrow mount, n. Focal length 1m. Curved slit. Dispersion, 5Å mm^{-1} in UV, 7.5Å mm^{-1} in visible. 1952: Two spectrographs, n, one for UV, the other for visible. Circular slits.	Pic du Midi, France; Khartoum, Sudan	Analysis of observations made by Lyot (1939) and Lyot and Aly (Lyot and Dollfus 1953), giving classifications derived from spatial distributions of line intensities and comparing these with identifications and ionisation potentials of Edlén (1942).
G Doschek et al (1975)	May 1973 to February 1974	Flares	970 - 3940Å	S082B spectrograph.	Skylab NRL/ATM	Identification of iron forbidden lines, with discussion of temporal variation of widths and intensities for 15 June 1973.
J Jefferies et al (1971)	30 May 1965	Corona during eclipse	3000-10800Å	Newtonian telescope with plane grating spectrograph, n. Circular slit. Dispersion, 36Å mm^{-1}. Spec res, 1Å. Spat res, 8".	Bellingshausen Island, French Polynesia	Identifications, classifications and absolute intensities at positions around the limb given.
K Kastner et al (1974)	24,25,26,27 February 1969 12 March 1969	Flares	65 - 170Å	Concave grating spectrometer, g. Detector scans 25 -400Å in 15 mins. r = 1m, i = 88˘, 576 lines mm^{-1}.Estimated spec res, 0.25Å.	OSO-5 satellite	List of solar flare lines, classified according to enhancement and with some identifications.
M Malinovsky and Heroux (1973)	4 April 1969	Moderately active disc	50 - 300Å	Double concave grating spectrometer, g. 4 detectors each scan, first deck, 45-325Å in 100s; second deck, intervals in range 180-1300Å in 50s. r = 2m, i = 86˘, 1200 lines mm^{-1}; 300 lines mm^{-1}. Spec res, 0.25Å; 0.8Å.	Aerobee 150 rocket from WSMR	List of identified lines presented with energy fluxes. Solar abundances determined.

TABLE 1 (continued)

Reference	Dates of Observations	Observed Solar Feature	Wavelength Range	Spectroscopic Instrument	Location of Instrument	Summary of Results
N Manson (1972)	3 November 1965; 8 August 1967	Very quiet disc; moderately active disc	30 - 128Å	Concave grating spectrometer, g. Detector scans 30 - 128Å in 100s. r = 2m, i = 86˚, 2400 lines mm^{-1}.Spec res., 0.21Å; 0.12Å	Aerobee 150 rocket from WSMR	Comparison of absolute intensities of spectra of a very quiet and an active sun.
O Neupert (1971)	23 May 1967	Flare	20 - 400Å	Concave grating spectrometer,g. Detector scans 20 - 400Å in 16 or 32 min or 6 intervals, 4Å wide, in 3min. r = 1m, i = 88˚, 576 lines mm^{-1}. Spec res., 0.6Å	OSO-III satellite	Discussion of solar flare X-ray and XUV spectra
P Noyes (1972)	23 August 1969	Flare	285 - 1385Å	Concave grating spectrometer-spectroheliometer, n. Grating scans 285 - 1385Å in 16 min or monitors intensity of single line every 80 ms. In spectroheliometer mode, entrance slit scans large, 45' x 45', or small, 6.8' x 7.9', raster in 8 min or 30s. Grating: r = 50cm, 1800 lines mm^{-1}. Telescope: 50 cm focal length. Spec res., 3Å. Spat. res., 35" x 35".	OSO-6 satellite	Discussion of solar flare XUV spectra.
Q Pecker et al (1954)	2 February 1950	Corona	Visible	Coronograph equipped with plane grating spectrograph, employing Littrow mount, n. Focal length 2.1m. Curved slit. 600 lines mm^{-1}. Spec res,0.3Å	Climax, Colorado, USA	Study of Ca XV lines at 5694.4 and 5446.5Å.
R Purcell and Widing (1972)	4 November 1969	Flare	170 - 670Å	Slitless, concave grating spectroheliograph, n. Grating rotated to select ranges 170 - 400Å and 370 - 670Å. r = 2m, 2400 lines mm^{-1}. Spec res, 0.2Å Spat res, ~ 5"	Aerobee 150 rocket from WSMR	Identifications of transitions in high ionisation stages of Ar, Ca and Fe, with discussion of Ar solar abundance and estimate of flare electron density.
S Sandlin et al (1976)	15 June, 9 August 1973	Flares	171 - 630Å	S082A spectrograph	Skylab NRL/ATM	List of high temperature flare lines, with identifications.
T Sandlin et al (1977)	May 1973 to February 1974	Limb including flares	974 - 2700Å	S082B spectrograph	Skylab NRL/ATM	List of coronal and transition zone lines, with identifications. Non-thermal velocities determined.
U Vernazza and Reeves (1978)	May 1973 to February 1974	Quiet and active regions, coronal holes, off-limb corona	277 - 1356Å	Concave grating spectrometer - spectroheliometer, n. 7 channel detector. Primarily first channel used in spectrometer mode, in which grating scans in 3.5 mins. In spectroheliometer mode, telescope mirror scans area 5' x 5' in 5.5 mins. Grating: r = 498.1 mm, 1800 lines mm^{-1}. Telescope: 2.3 m focal length. Spec res,1.6Å, Spat res,5" x 5".	Skylab Harvard/ATM	Identifications and absolute line intensities given for composite XUV spectrum for various solar features. Discussion includes calculation of electron densities and comparison with quiet sun spectrum at solar maximum.
V Waldmeier (1951)	21 February 1942 25 July 1947 26 March 1949 31 August 1949 9 July 1950	Corona	4800 - 6000Å 5600 - 8000Å	Coronograph equipped with prism spectrograph, using Amici prism systems. Focal length 1.5m. Straight slit. Dispersion, 9Åmm^{-1} at 5303Å, 23Åmm^{-1} at 6374Å	Arosa, Switzerland	Observations and tentative identification of the Ca XV line at 5445Å.

TABLE 1 (continued)

Reference	Dates of Observations	Observed Solar Feature	Wavelength Range	Spectroscopic Instrument	Location of Instrument	Summary of Results
W Widing (1975)	15 June, 9 August 1973	Flares	171 - 630Å	S082A spectrograph	Skylab NRL/ATM	Identifications and measurements of beryllium-like lines, including a discussion of the Fe XXIII, 263Å and Fe XXIV, 255Å observations.
X Widing (1978)	May 1973 to February 1974	Flares	320 - 600Å	S082A spectrograph	Skylab NRL/ATM	List of high temperature flare lines, with identifications of iron and nickel forbidden transitions. Particular attention given to flare of 17 December 1973.
Y Widing and Purcell (1976)	4 November 1969; 9 August, 17 December 1973 15 January 1974	Flares	171 - 630Å	As R; S082A spectrograph	As R; Skylab NRL/ATM	Identifications and wavelength measurements of lithium-like lines, with comparison with atomic structure theory.

ATM - Apollo Telescope Mount
g - Grazing incidence instrument
i - Angle of incidence of radiation falling on grating
n - Normal incidence instrument
OSO - Orbiting solar observatory
r - Radius of curvature of grating
WSMR- White Sands Missile Range, New Mexico, USA

TABLE 2. Classifications of solar observations isoelectronic with fluorine I (Nomenclature and abbreviations explained in Table 9)

Transition	Calculated wavelength	Solar observations				
Ca XII						
$2s^22p^5$ - $2s2p$						
$^2P_{3/2}$ - $^2S_{1/2}$	141.036	A 141.032(30)a				
$^2P_{1/2}$ - $^2S_{1/2}$	147.278	A 147.274(25)a				
$2s^22p^5$						
($^2P_{3/2}$ - $^2P_{1/2}$)	3326.34	F 3329.6 (Group 6702A)f	J 3327.5 (III 0.36 0.53)j			
	(3327.30)	(3330.6)	(3328.5)			
Fe XVIII						
$2s^22p^5$ - $2s2p^6$						
$^2P_{3/2}$ - $^2S_{1/2}$	93.923	A 93.933(20)	K 93.94bl (220 104III)k	M 93.93bl (0.7)m	N 93.97 (6.8)	Blend with Fe X, $3p^5\,^2P_{3/2}$ - $3p^4(^1D)4s\,^2D_{5/2}$ at 94.012A and Fe XX, $2s^22p^3\,^2D_{5/2}$ - $2s2p^4\,^2P_{3/2}$ - see text
$^2P_{1/2}$ - $^2S_{1/2}$	103.937	A 103.928(30W)	K 103.954 (111 75III)k	M 103.95bl(2.0)m	N 103.94 (4.9)	Blend with unidentified quiet sun line at 103.89A
$2s^22p^5$						
($^2P_{3/2}$ - $^2P_{1/2}$)	974.85	G 974.8g	T 974.86 ± 0.05t			

Wavelengths given in A
Wavelengths above 2000A are in air (vacuum wavelengths are given in brackets)
bl denotes blend
Upper case letters indicate observations and lower case identifications. The key is given in Table 9.
Intensities and temperature classifications, given in brackets after the wavelengths, are explained in Table 9.

TABLE 3. Classifications of solar observations isoelectronic with oxygen I

Transition	Calculated wavelength	Solar observations	Blends
Ca XIII			
$2s^22p^4$			
$(^3P_2 - {}^1D_2)$	1133.66	D 1133.68?	
$(^3P_2 - {}^3P_1)$	4087.0 (4088.1)	F 4086.5 (Group 6702Å)f J 4087.1 (III 1.65 0.80)j (4087.7) (4088.3)	
Fe XIX			
$2s^22p^4 - 2s2p^5$			
$^1D_2 - {}^1P_1$	91.015	K 91.21 (42 40 III)k?	If present, blend with Fe XXI, $2s^22p^2{}^3P_0 - 2s2p^3{}^3S_1$, and, possibly, with quiet/active sun line at 90.96/91.004Å
$^3P_2 - {}^3P_1$	101.548	K 101.55 (82 77 IV)k	Possibly blend with quiet/active sun line at 101.55/101.559Å
$^3P_1 - {}^3P_0$	106.317	K 106.28 (30 31 II)k	Blend, probably with Ne VII, $2s2p^3P_2 - 2s3d^3D_3$ at 106.192Å
$^3P_2 - {}^3P_2$	108.353	K 108.37 (283 160 III)k	Possibly contains component of Fe XXI, $2s^22p^2{}^3P_0 - 2s2p^3{}^3P_1$
$^3P_0 - {}^3P_1$	109.951	K 110.14 (56 34 IV) k	
$^3P_1 - {}^3P_1$	111.692	K 111.80 (70 71 IV) k	Possibly blend with Mg VI, $2s^22p^3{}^4S_{3/2} - 2s^22p^2(^3P)3s^4P_{3/2}$ at 111.746Å
$^3P_1 - {}^3P_2$	119.980	K 119.92 (110 72 IV) k	
$2s^22p^4$			
$(^3P_1 - {}^1S_0)$	424.25	S 424.24 (I-II 6) X 424.26 (III 14)x	
$(^3P_2 - {}^1D_2)$	592.21	E 592.24 (6) e S 592.24 (I 7) X 592.16 (III 22?)x	
$(^3P_2 - {}^3P_1)$	1118.08	D 1118.10 d G 1118.1 ± 0.1g T 1118.07 ± 0.05t	
Ni XXI			
$2s^22p^4$			
$(^3P_2 - {}^1D_2)$	471.16	S 471.10 (I-II 5) X 471.15 (IV 6)x	

Wavelengths given in Å
Wavelengths above 2000Å are in air (vacuum wavelengths are given in brackets)
bl denotes blend
? indicates a tentative identification or uncertain intensity.
Upper case letters indicate observations and lower case identifications. The key is given in Table 9.
Intensities and temperature classifications, given in brackets after the wavelengths, are explained in Table 9.

TABLE 4. Classifications of solar observations isoelectronic with nitrogen I

Transition	Observed or calculated wavelength	Solar observations	Blends
Ca XIV			
$2s^22p^3 - 2s2p^4$			
$^4S_{3/2} - {}^4P_{1/2}$	183.45	E 183.45 (3)e R 183.42r	
$^4S_{3/2} - {}^4P_{3/2}$	186.60	A 186.609bl(40)a B 186.605(5)b E 186.60(3)e R 186.60r	Blend with Fe VIII, $3p^63d^2D_{3/2} - 3p^53d^2(^3F)^2F_{5/2}$ at 186.599A
$^4S_{3/2} - {}^4P_{5/2}$	193.86	A 193.880 (20)a B 193.872 b E 193.87(2)e R 193.88r	
Fe XX			
$2s^22p^3 - 2s2p^4$			
$^2D_{5/2} - {}^2P_{3/2}$	93.79	K 93.94 (220 104 III)1	Blend with Fe XVIII, $2s^22p^{5\,2}P_{3/2} - 2s2p^{6\,2}S_{1/2}$
$^2D_{3/2} - {}^2D_{3/2}$	110.64	K 110.86 (36 36 IV)	
$^2D_{5/2} - {}^2D_{5/2}$	113.35	K 113.45 (54 27 IV)k	Possibly blend with Fe XXI, $2s^22p^{21}D_2 - 2s2p^{31}D_2$
$^4S_{3/2} - {}^4P_{1/2}$	118.66	K 118.70 (201 165 IV)k	Possibly blend with Fe XXI, $2s^22p^{23}P_1 - 2s2p^{33}P_0$
$^4S_{3/2} - {}^4P_{3/2}$	121.83	K 121.85 (203 225 IV)h	Possibly blend with quiet/active sun line at 121.74/121.79A
$^4S_{3/2} - {}^4P_{5/2}$	132.85	K 132.83 (- 2330 IV)h	Blend with intense Fe XXIII, $2s^{21}S_0 - 2s2p^1P_1$
$2s^22p^3$			
$(^4S_{3/2} - {}^2P_{3/2})$	309.27	E 309.24 (-) S 309.26 (I 3)	
$(^2D_{3/2} - {}^2P_{3/2})$	541.33	X 541.35 (III-IV 13)x	
$(^4S_{3/2} - {}^2D_{5/2})$	567.78	E 567.85(6) S 567.81 (I-II 8) X 567.76 (IV 40)	

Wavelengths given in A
bl denotes blend
Upper case letters indicate observations and lower case identifications. The key is given in Table 9.
Intensities and temperature classifications, given in brackets after the wavelengths, are explained in Table 9.

TABLE 5. Classifications of solar observations isoelectronic with carbon I

Transition	Observed or calculated wavelength	Solar observations	Blends
Ca XV			
$2s^22p^2$ - $2s2p^3$			
$^3P_1$ - $^3P_1$	176.91	E 176.95 (-)	Blend with active sun line at 176.982A
$^3P_1$ - $^3P_0$	177.25	E 177.24 (4)?	If present, blended with Fe X, $3p^5\,^2P_{3/2}$ - $3p^4(^1D)3d\,^2P_{3/2}$ at 177.243A
$^3P_2$ - $^3P_2$	181.90	E 181.91 (-)e S 181.93 (I 5)s	
$^3P_0$ - $^3D_1$	200.96	E 200.98 (-)e S 200.92bl r S 201.02 (I 2)s	Blend, possibly with Fe XIII, $3p^2\,^3P_1$ - $3p3d\,^3D_1$ at 201.134A
$^3P_1$ - $^3D_1$	208.31	E 208.33bl(-)e	Blend with S X, $2s^22p^3\,^2P_{3/2}$ - $2s2p^4\,^2S_{1/2}$ at 208.322A
$^3P_1$ - $^3D_2$	208.71	E 208.70 (-)e R 208.69 r S 208.72 (I 3)s	Possibly blend with Fe XIII, $3p^2\,^1S_0$ - $3p3d\,^1P_1$ at 208.679A
$^3P_2$ - $^3D_3$	215.37	E 215.38 (3)e R 215.48 r S 215.38 (I 4)s	
$^3P_1$ - $^5S_2$	383.8	E 382.84 (6)? X 382.82(II 11)?	Blend with Fe XII, $3s^23p^3\,^2P_{3/2}$ - $3s3p^4\,^2D_{5/2}$ at 382.83A
$^3P_2$ - $^5S_2$	412.9	E 411.65 (5)? S 411.55(I 5)? X 411.61 (II? 10?)?	Blend with Ca X, $3p^2\,^2P_{1/2}$ - $3d^2\,^2D_{3/2}$ at 411.690A
$2s^22p^2$			
($^3P_2$ - $^1D_2$)	1375.88	D 1375.91 (30) T 1375.95 ± 0.03 (VI 0.04)t	Possibly blend with Ni II, $3d^8(^3P)4s^2\,^2P_{3/2}$ - $3d^7(^4F)4s4p(^3P)\,^2D_{5/2}$ at 1375.822A
($^3P_1$ - $^3P_2$)	5445.1	F 5444.5 (Group 5694A)f J 5444 (IV - -)j Q 5446.5 (1)q	
	(5446.6)	(5446.0) (5446) (5448.0)	
		V 5445.2v	
		(5446.7)	
($^3P_0$ - $^3P_1$)	5694.8	F 5694.5 (Group 5694A)f J 5693.6(IV 0.21-)j Q 5694.4(1.6)q	
	(5696.4)	(5696.1) (5695.2) (5696.0)	
Fe XXI			
$2s^22p^2$ - $2s2p^3$			
$^3P_0$ - $^3S_1$	91.28	K 91.21 (42 40 III)l?	If present, blended with Fe XIX, $2s^22p^4\,^1D_2$ - $2s2p^5\,^1P_1$
$^3P_1$ - $^3S_1$	97.88	I 97.88 (? 68 III)i?	If present, blended with Fe X, $3p^5\,^2P_{3/2}$ - $3p^4(^3P)4s^4P_{5/2}$ at 97.838A
$^3P_2$ - $^3S_1$	102.22	K 102.35 (111 110 IV)i	Blend with unreported line and, possibly, with quiet/active sun line at 102.10/102 A
$^3P_0$ - $^3P_1$	108.12	K 108.37 (283 160 III)l?	If present, blended with Fe XIX, $2s^22p^4\,^3P_2$ - $2s2p^5\,^3P_2$ and, possibly, with Fe VIII, $3d^2D_{5/2}$ - $5f^2F_{7/2}$ at 108.083A
$^3P_1$ - $^3P_1$	117.51	K 117.81 (129bl 115 III)l	Blend with Ni XXV, $2s^2\,^1S_0$ - $2s2p\,^1P_1$ - see text
$^3P_1$ - $^3P_0$	118.69	K 118.70 (201 165 IV)l?	If present, blended with Fe XX, $2s^22p^3\,^4S_{3/2}$ - $2s2p^4\,^4P_{1/2}$
$^3P_2$ - $^3P_2$	121.21	K 121.17 (- 34 III)l	
$^3P_2$ - $^3P_1$	123.82	K 123.76 (48 48 III)k?	If present, blended - nearest reported solar line at 123.492A
$^1D_2$ - $^1D_2$	113.30	K 113.45 (54 27 IV) l?	If present, blended with Fe XX, $2s^22p^3\,^2D_{5/2}$ - $2s2p^4\,^2D_{5/2}$
$^3P_0$ - $^3D_1$	128.73	K 128.74 (90 712 IV) h	
$^3P_1$ - $^3D_2$	142.16	K 142.18 (15 94 III)l	Blended with Fe XXI, $2s^22p^2\,^3P_1$ - $2s2p^3\,^3D_1$
$^3P_1$ - $^3D_1$	142.26	K 142.18 (15 94 III)	Blended with Fe XXI, $2s^22p^2\,^3P_1$ - $2s2p^3\,^3D_2$
$^3P_2$ - $^3D_3$	145.65	K 145.66 (- 45 IV)l	Possibly blend with a weak active sun line at 145.656 A
$^3P_1$ - $^5S_2$	242.06	E 242.07 (4)e S 242.07 (II 5)	
$^3P_2$ - $^5S_2$	270.47	E 270.52 bl(-)e	Blend with Fe XIV, $3s^23p^2\,^2P_{3/2}$ - $3s3p^2\,^2P_{1/2}$ at 270.512A
$2s^22p^2$			
($^3P_0$ - $^3P_1$)	1354.06	C 1354.04 ± 0.05c D 1354.14d G 1354.1 ± 0.1g	
		T 1354.08 ± 0.05t	

Wavelengths given in Å
Wavelengths above 2000A are in air (vacuum wavelengths are given in brackets)
bl denotes blend
? indicates a tentative identification or uncertain classification or intensity
Upper case letters indicate observations and lower case identifications. The key is given in Table 9.
Intensities and temperature classifications, given in brackets after the wavelengths, are explained in Table 9.

TABLE 6. Classifications of solar observations isoelectronic with boron I

Transition	Calculated wavelength	Solar observations	Blends
Ca XVI			
$2s^22p - 2s2p^2$			
$^2P_{3/2} - {}^2P_{3/2}$	164.158	A 164.146 (35)? B 164.13(5)? K 164.14 (121 127 II)	Probably blend with Ni XIV, $3s^23p^3{}^2D_{5/2} - 3s^23p^2\ (^1D)3d^2F_{7/2}$ at 164.146A
$^2P_{3/2} - {}^2P_{1/2}$	167.430	K 167.50 (119 129 I)?	If present, blended with Fe VIII, $3p^63d^2D_{3/2} - 3p^53d^2(^3F)\ ^2D_{3/2}$ at 167.495A
$^2P_{1/2} - {}^2D_{3/2}$	208.585	E 208.59(3)e R 208.69bl r S 208.59 (I, 6)s	Blend with active sun line at 208.690A
$^2P_{3/2} - {}^2D_{5/2}$	224.522	E 224.54(2)e S 224.54 (I, 5)s	
$^3P_{3/2} - {}^2D_{3/2}$	225.832	E 225.87(-)e R 225.96bl r S 225.85 (I, 2)s	Blend with active sun line at 225.867A
Fe XXII			
$2s^22p - 2s2p^2$			
$^2P_{1/2} - {}^2P_{3/2}$	100.768	K 100.89 (51 52 II)l?	If present, blended, probably with quiet/active sun line at 101.01/100.96A
$^2P_{3/2} - {}^2P_{3/2}$	114.401	K 114.41 (142 115 IV)h	Blend-nearest reported line Mg V, $2s^22p^4{}^3P_2 - 2s^22p^3\ (^2D)\ 3d^3P_2$ at 114.036A
$^2P_{1/2} - {}^2S_{1/2}$	117.151	K 117.18 (513 568 III)k	Possibly blend with quiet/active sun line at 117.15/117.20A
$^2P_{1/2} - {}^2D_{3/2}$	135.761	K 135.73 (298 655 IV)k	
$^2P_{3/2} - {}^2D_{5/2}$	155.931	K 155.89 (48 63 -)	
$^2P_{1/2} - {}^4P_{3/2}$	217.29	E 217.28 (-) S 217.30 (II-III?1)s	Blend with Fe XII, $3p^3{}^2D_{3/2} - 3p^2(^3P)3d^2P_{3/2}$ at 217.271A
$^2P_{1/2} - {}^4P_{1/2}$	247.16	E 247.18 bl(4)e S 247.19 (III 5)s	Blend with N IV, $2s^21S_0 - 2s3p^1P_1$ at 247.205A and, possibly, with S XI, $2s^22p^23P_2 - 2s2p^33P_1$ at 247.16A
$^2P_{3/2} - {}^4P_{5/2}$	253.16	E 253.17 (4)e S 253.17 (III 5)s	
$^2P_{3/2} - {}^4P_{3/2}$	292.45	E 292.48(4)e S 292.46 (III 5)s	
$^2P_{3/2} - {}^4P_{1/2}$	349.26	E 349.13(7) S 349.3 bl (I-III < 6)s	Blend with Mg VI, $2s^22p^3{}^2D_{5/2} - 2s2p^4{}^2D_{5/2}$ at 349.155A
$2s^22p$			
$(^2P_{1/2} - {}^2P_{3/2})$	845.63	P 845.4 ± 0.2p	
Ni XXIV			
$2s^22p - 2s2p^2$			
$^2P_{1/2} - {}^2S_{1/2}$	104.592	K 104.60 (34 45 IV)	

Wavelengths given in A
bl denotes blend
? indicates a tentative identification or uncertain classification.
Upper case letters indicate observations and lower case identifications. The key is given in Table 9.
Intensities and temperature classifications, given in brackets after the wavelengths, are explained in Table 9.

TABLE 7. Classifications of solar observations isoelectronic with beryllium I

Transition	Calculated wavelength	Solar observations	Blends
Ca XVII			
$2s^2$ - 2s2p			
$^1S_0$ - $^1P_1$	192.858	E 192.86(5)e R 192.88 r S 192.85(I 8)s W 192.87 w	Possibly blend with Fe XI, $3p^4\,^3P_1$ - $3p^3(^2P)3d\,^3P_2$ at 192.819A
$^1S_0$ - $^3P_1$	371.037	E 371.04(7)e S 371.11(I 5)s U 371.4 u? W 371.06 w X 371.04 (II 14)x	
2s2p - $2p^2$			
$^3P_2$ - $^3P_2$	232.812	E 232.81(2)e S 232.81(I 4)s	
Cr XXI			
$2s^2$ - 2s2p			
$^1S_0$ - $^3P_1$	293.166	E 293.15(3)e S 293.16(III 3)s W 293.11 w	
Mn XXII			
$2s^2$ - 2s2p			
$^1S_0$ - $^1P_1$	141.091	K 141.14 (42 63 IV)?	Possibly blend with Ca XII, $2s^22p^5\,^2P_{3/2}$ - $2s2p^6\,^2S_{1/2}$
$^1S_0$ - $^3P_1$	277.823	E 277.75 (-)e S 277.80 (III 2)s	
Fe XXIII			
$2s^2$ - 2s2p			
$^1S_0$ - $^1P_1$	132.869	K 132.83 (- 2330 IV)k	Blend with Fe XX, $2s^22p^3\,^4S_{3/2}$ - $2s2p^4\,^4P_{5/2}$
$^1S_0$ - $^3P_1$	263.740	E 263.76(5)e S 263.74 (III 8)s W 263.76 w	
Ni XXV			
$2s^2$ - 2s2p			
$^1S_0$ - $^1P_1$	117.947	K 117.81 (129 bl 115 III)	Blend with Fe XXI, $2s^22p^2\,^3P_1$ - $2s2p^3\,^3P_1$ - see text

Wavelengths given in A
bl denotes blend
? indicates a tentative identification.
Upper case letters indicate observations and lower case identifications. The key is given in Table 9.
Intensities and temperature classifications, given in brackets after the wavelengths, are explained in Table 9.

TABLE 8. Classifications of solar observations isoelectronic with lithium I

Transition	Calculated wavelength	Solar observations	Blends
Ca XVIII			
2s - 2p			
$^2S_{1/2}$ - $^2P_{3/2}$	302.215	E 302.21(8)e R 302.22 r S 302,20 (I, 9)s Y 302.19 y	
$^2S_{1/2}$ - $^2P_{1/2}$	344.780	E 344.75 (6,8)e R 344.80 r S 344.80 (I, 9)s X 344.74 (III 53)x Y 344.76 y	
Ti XX			
2s - 2p			
$^2S_{1/2}$ - $^2P_{3/2}$	259.296	E 259.26 (5)e S 259.24 (IV 2)s	
Cr XXII			
2s - 2p			
$^2S_{1/2}$ - $^2P_{3/2}$	223.015	E 222.99(2)e S 222.99 (IV 6)s Y 223.00 y	Possibly blend with active sun line at 223.004Å
$^2S_{1/2}$ - $^2P_{1/2}$	279.712	E 279.70(3)e S 279.69 (IV 5)s Y 279.69 y	
Mn XXIII			
2s - 2p			
$^2S_{1/2}$ - $^2P_{3/2}$	206.921	E 206.87(-)e S 206.89 (IV 3)s Y 206.90 y	
$^2S_{1/2}$ - $^2P_{1/2}$	266.882	E 266.86(-)e S 266.88 (IV 3)s Y 266.88 y	
Fe XXIV			
2s - 2p			
$^2S_{1/2}$ - $^2P_{3/2}$	192.017	E 192.03 (4)e O 191 (2)o R 192.14 r S 192.03 (IV 9)s Y 192.04y	
$^2S_{1/2}$ - $^2P_{1/2}$	255.095	E 255.11 (6)e O 255.1(1)o R 255.29 r S 255.10 (IV 9)s Y 255.10y	
Ni XXVI			
2s - 2p			
$^2S_{1/2}$ - $^2P_{3/2}$	165.378	K 165.42 (70 78 III) y	Possibly blend with Ar X, $2s^22p^5{}^2P_{3/2}$ - $2s2p^6{}^2S_{1/2}$ at 165.509Å.
$^2S_{1/2}$ - $^2P_{1/2}$	234.196	S 234.20 (IV 4)s Y 234.20 bl y	Blend with He II, $1s^2S_{1/2}$ - $6p^2P_{3/2}$ at 234.347Å

Wavelengths given in Å
bl denotes blend
Upper case letters indicate observations and lower case identifications. The key is given in Table 9.
Intensities and temperature classifications, given in brackets after the wavelengths, are explained in Table 9.

TABLE 9 Notation used in tables 2-8

Reference	Remarks including explanation of intensities, classifications and other notation
A Behring et al (1972)	Visual intensity estimate given on scale 20-90. W indicates that a line is wide
B Behring et al (1976)	Approximate relative intensities given for some lines on scale 1-500, 500 corresponding to the He II, 303.782Å line.
C Cheng et al (1979)	Wavelength accuracy reported.
D Cohen et al (1978)	Absolute intensities of the line peaks, in ergs $cm^{-2}s^{-1}sr^{-1}Å^{-1}$, are presented for many lines.
E Dere (1978)	Relative intensities are on a scale from 1 to 10. They are derived from the maximum photographic density on the short and long wavelength plates exposed at 1554 and 1555 UT, respectively, during the 9 August 1973 flare.
F Dollfus (1957)	Lines classified into groups, denoted by the strongest line in the group and determined from the spatial distribution of the line intensities. Classifications are found to be consistent with those by ionisation potential.
G Doschek et al (1975)	Two wavelength accuracies reported.
H Fawcett and Cowan (1975)	Only identifications made.
I Feldman (1976)	An additional observation from the spectra of K reported. Notation is as for K.
J Jefferies et al (1971)	Classification using the Lyot-Shajn scheme as in F: class I, group 6374Å; class II, group 5303Å; class III, group 6702Å; class IV, group 5694Å. Absolute intensities measured in a coronal condensation in units of erg $cm^{-2}s^{-1}sr^{-1}$ are presented for two heights above the limb, the first being the lower.
K Kastner et al (1974)	Relative intensities, being the number of counts in 0.30s, are given for two flares, the first intensity for flare E observed on 12 March 1969 and the second for flare B on 25 February 1969. Classifications represent the degree of enhancement above quiet sun intensities: type I, enhancement of less than 2; type II, between 2 and 5; type III, between 5 and 20; type IV new flare line.
L Kononov et al (1976a)	No solar observations reported, only identifications of solar lines being made.
M Malinovsky and Heroux (1973)	Absolute line intensities, in units of 10^{-3} ergs $cm^{-2}s^{-1}$, are presented.
N Manson (1972)	The photon flux is given in units of 10^6 photons $cm^{-2}s^{-1}$.
O Neupert (1971)	Intensities represent an approximate intensity ratio for the listed lines.
P Noyes (1972)	Wavelength accuracy given.
Q Pecker et al (1954)	An intensity ratio is given for the listed lines.
R Purcell and Widing (1972)	No intensities or classifications included.
S Sandlin et al (1976)	Lines classified according to temperature: class I, log T_e = 6.5 - 7.0; class II, 7.0 - 7.1; class III, 7.1 - 7.2; class IV, 7.2 - 7.3. Visual estimates of relative peak intensities on a scale from 1 to 10 given for the flare of 9 August 1973.
T Sandlin et al (1977)	Wavelength accuracies noted. Where given temperature classification is as follows: class IV, log T_e = 5.6 - 5.9; class V, 5.9 - 6.1; class VI, $\geqslant$ 6.1. Intensities are relative, being measured on a scale from 0 to 10 on the limb above an active region.
U Vernazza and Reeves (1978)	Only wavelengths are taken from this reference.
V Waldmeier (1951)	A similarity is noted between the appearance and behaviour of the Ca XV lines at 5445 and 5694Å.
W Widing (1975)	No intensities or classifications included.
X Widing (1978)	Classifications are according to temperature: class I, $T_e \lesssim 4 \times 10^6$K; class II, 4-7 x 10^6K; class III, 7-10 x 10^6K, class IV, $\geqslant 10^7$K. Relative intensities are from the flare of 17 December 1973. Those for the longer wavelengths are underestimated because of image aberrations.
Y Widing and Purcell (1976)	No intensities or classifications given.

CLM - P 693

CLM - P 693

UKAEA

Preprint

THE EFFECT OF A RELATIVISTIC RESONANCE CONDITION ON THE FOKKER-PLANCK THEORY OF ECRH CURRENT DRIVE

D. F. H. START
M. R. O'BRIEN
P. M. V. GRACE

CULHAM LABORATORY
Abingdon Oxfordshire

1983

CLM-P693

THE EFFECT OF A RELATIVISTIC RESONANCE CONDITION ON THE FOKKER-PLANCK THEORY OF ECRH CURRENT DRIVE

D F H Start, M R O'Brien and P M V Grace*
Culham Laboratory, Abingdon, Oxon, OX14 3DB, UK
(Euratom/UKAEA Fusion Association)
*St John's College, Cambridge, UK.

ABSTRACT

The efficiency of current drive by X-mode electron cyclotron waves is calculated using the weakly relativistic resonance condition in a full Fokker-Planck treatment which includes electron-electron collisions. For suprathermal resonant electrons the values obtained are less by a factor (Z+5)/Z than those predicted by the Lorentz gas model. However this relationship is found not to hold for resonant parallel velocities less than the thermal velocity. A ray tracing code, incorporating the calculated current drive efficiencies, has been used to study the relativisitic corrections for X-mode second harmonic waves injected from the low field side into a tokamak the size of DITE.

(Submitted for publication in Plasma Physics)

May 1983

1 INTRODUCTION

The non-inductive current drive scheme using electron cyclotron resonance heating (ECRH) relies on preferentially heating electrons which are moving in one direction along the magnetic field lines [1]. This can be achieved by tuning the wave frequency ω such that the Doppler shift due to the electron velocity along the magnetic field synchronises the wave frequency and the electron gyrofrequency or one of its harmonics. Thus for non-relativistic electrons, resonance is achieved for all perpendicular velocities provided the parallel velocity $v_{\parallel}$ satisfies the condition $(\omega-\ell\Omega) = k_{\parallel} v_{\parallel}$, where $k_{\parallel}$ is the parallel wave vector, Ω is the electron gyrofrequency and ℓ is the harmonic number. Electrons moving parallel (antiparallel) with the wave will be in resonance if the wave frequency is greater (less) than $\ell\Omega$. In the inhomogeneous field of a tokamak the frequency difference $(\omega-\ell\Omega)$ changes sign across the resonance layer so that the current flows in opposite directions on opposite sides of the resonance. For a weakly absorbed wave these opposing currents are of equal amplitude and no net current flows.

As the electrons become relativistic the gyrofrequency develops a velocity dependence due to the relativistic mass increase. This velocity dependence can affect both the absorption profiles[2 3] and, as shown in a recent paper by Cairns, Owen and Lashmore-Davies[4], can substantially change and enrich the phenomenology of ECRH current drive. The principal effect is that the current is no longer an antisymmetric function of $(\omega-\ell\Omega)$ where Ω is the non-relativistic gyrofrequency. Thus in a tokamak the currents on opposite sides of the cyclotron resonance layer have different amplitudes and do not cancel in the case of weak absorption.

The calculations in ref 4 used a simplified collision operator which neglected electron-electron collisions. In the present paper we include these collisions in a full Fokker-Planck treatment for X-mode cyclotron waves of arbitrary harmonic number ℓ. The results have been incorporated into a ray tracing code which is used to compare the relativistic and non-relativistic calculations in a practical application. For this we have chosen the example of second harmonic X-mode RF injected into a tokamak similar to DITE.

2 THE RESONANCE CONDITION

The electron cyclotron resonance condition for mildly relativistic electrons can be written

$$k_{\parallel} v_{\parallel} = \omega - \ell\Omega \left(1 - \frac{v_{\parallel}^2+v_{\perp}^2}{2c^2}\right) \qquad (1)$$

where c is the velocity of light and $v_{\parallel}$ and $v_{\perp}$ are the electron parallel and perpendicular velocities respectively. In terms of normalised velocity space co-ordinates, $v_{\parallel}/v_e$ and $v_{\perp}/v_e$, the resonance condition is a semicircle of radius $(1-4u_o S)^{\frac{1}{2}}/2S$ centred on the $v_{\perp}/v_e=0$ axis at $v_{\parallel}/v_e = (2S)^{-1}$. The parameters u_o and S are defined by $u_o=(\omega-\ell\Omega)/k_{\parallel} v_e$ and

$S=\ell\Omega v_e/(2k_\parallel c^2)$ and the electron thermal velocity, v_e, is related to the temperature, T_e, by $v_e^2 = 2T_e/m$, where m is the electron mass. In the non-relativistic limit the resonance becomes the straight line $v_\parallel/v_e = u_o$. Several resonance curves for positive values of S are shown in Fig 1 for both $u_o = 1$ and $u_o = -1$. For $S > 0$, positive values of u_o correspond to absorption on the low field side of the ECR in a tokamak. In this case the mass increase serves to increase the difference between the wave frequency and the gyrofrequency leading to resonant values of $v_\parallel$ which are always positive and greater than the non-relativistic value. Note that for $S > (4u_o)^{-1}$ the frequency difference cannot be recovered by the Doppler shift for any value of $v_\parallel$ and so a cut-off in the wave absorption occurs. At cut-off the resonance semi-circle collapses to a point at $v_\parallel/v_e = 2u_o$, $v_\perp/v_e = 0$.

On the high field side of the ECR the gyrofrequency exceeds the wave frequency for non-relativistic electrons and the resonance condition is satisfied by negative values of $v_\parallel$. However for sufficiently energetic electrons the mass increase causes the gyrofrequency to fall below the wave frequency giving rise to positive values of $v_\parallel$ at resonance as shown in Fig 1. Thus on the high field side electrons moving both parallel and antiparallel to the wave can absorb power. For propagation of the wave perpendicular to the magnetic field ($k_\parallel = 0$) all directionality disappears as expected and the wave is absorbed by iso-energetic electrons. The resonance curve is the zero-centred semicircle given by $v^2 = 2(\ell\Omega - \omega)c^2/(\ell\Omega)$.

3 THE FOKKER-PLANCK EQUATION

The linearised, steady state electron Fokker-Planck equation can be written as [5]

$$\frac{1}{v_\perp}\frac{\partial}{\partial v_\perp}\left\{ Dv_\perp \left(\frac{v_\perp}{v_e}\right)^{2(\ell-1)} \delta\left[\frac{\omega}{k_\parallel} - \frac{\ell\Omega}{k_\parallel}\left(1 - \frac{v^2}{2c^2}\right) - v_\parallel\right]\frac{\partial F_{me}}{\partial v_\perp}\right\} \qquad (2)$$

$$+ C_{ei}(f_e', F_{mi}) + C_{ee}(f_e', F_{me}) + C_{ee}(F_{me}, f_e') = 0$$

where the first term is the quasi-linear diffusion operator describing the effect of X-mode wave absorption, C represents the non-relativistic Fokker-Planck collision operator, and f_e' is the perturbation of the electron distribution function away from the Maxwellian F_{me}. The parameter D for the X-mode is independent of velocity space variables and is proportional to the square of the perpendicular electric field component which rotates in phase with the electrons. Using the Legendre polynomial representation of f_e', namely $f_e' = F_{me} \Sigma a_n P_n(v_\parallel/v)$, we find that the coefficient a_1, from which the current can be calculated, satisfies the integro-differential equation

$$a_1'' + P(x)\, a_1' + Q(x)\, a_1 - \frac{16}{3\pi^{\frac{1}{2}}\Lambda}\left[xI_3(x)-1.2xI_5(x)-x^4(1-1.2x^2)(I_o(x)-I_o(\infty))\right] = R(x) \tag{3}$$

where the dash denotes differentiation with respect to $x(=v/v_e)$. The terms on the left hand side are due entirely to the collisions while the term on the right hand side is due to the wave interaction and is given by

$$R(x) = \frac{12D}{v_e^3 \nu_o \Lambda}(x^2-x_o^2)^{\ell-1} x_o x\{x_o^2 + \ell - x^2 + [x^2-(2\ell+1)x_o^2]Sx_o^{-1}\}\{H(x-\alpha_-)-H(x-\alpha_+)\} \tag{4}$$

where $\alpha_\pm = \left|(1\pm\sqrt{1-4u_o S})/2S\right|$, $x_o=u_o+x^2S$, $\nu_o=e^4 n_e \ell n\lambda/4\pi\varepsilon_o^2 v_e^3 m^2$, $\Lambda=E-xE'$, H is the Heaviside function, n_e is the electron density, $\ell n\lambda$ is the Coulomb logarithm and E is the error function. In eqn (3) the functions P(x), Q(x) and $I_n(x)$ are those defined in ref 5, namely

$$P(x) = -x^{-1}-2x+2x^2E'/\Lambda \tag{5}$$

$$Q(x) = x^{-2}-2(Z+E-2x^3E')/\Lambda \tag{6}$$

$$I_n(x) = \int_o^x a_1(y)e^{-y^2}y^n dy \tag{7}$$

where Z is the effective plasma charge.

Note that a change of sign of $k_\parallel$ simultaneously reverses the signs of both u_o and S thereby changing the sign but not the magnitude of R(x). Physically this means that for a wave propagating through a tokamak plasma a reversal of the wave direction reverses the currents on each side of the resonance but leaves their magnitudes unchanged. Thus in the following calculations we shall keep $k_\parallel$ positive (S positive) and change the sign of u_o to investigate the low and high field sides of the resonance.

The electron current density J is given by

$$J = -e\int v_\parallel f_e' d^3v = -\frac{4e}{3\pi^{\frac{1}{2}}} v_e n_e I_3(\infty) \tag{8}$$

and the absorbed power density by

$$P_d = \tfrac{1}{2}m_e\int \frac{v^2}{v_\perp}\frac{\partial}{\partial v_\perp}\left\{Dv_\perp\left(\frac{v_\perp}{v_e}\right)^{2(\ell-1)}\delta\left[\frac{\omega}{k_\parallel}-\frac{\ell\Omega}{k_\parallel}\left(1-\frac{v^2}{2c^2}\right)-v_\parallel\right]\frac{\partial F_{me}}{\partial v_\perp}\right\}d^3v \tag{9}$$

Changing variables to x and $\xi = (v_\parallel/v)$ and integrating we obtain

$$P_d = 4Dn_e m_e G_\ell / (\pi^{\frac{1}{2}} v_e) \tag{10}$$

where $G_\ell = \int_{\alpha_-}^{\alpha_+} x^3 (x^2-x_o^2)^{\ell-1} (x^2-x_o^2-\ell+2\ell x_o S) e^{-x^2} dx$ (11)

Expressions for G_ℓ are given in the appendix for $\ell = 1$ and $\ell = 2$. In the usual units of $-nev_e$ for J and $nm_e v_e^2 \nu_o$ for P_d, the current drive efficiency J/P_d is given by

$$\frac{J}{P_d} = \frac{v_e^3 \nu_o}{3D} \cdot \frac{I_3(\infty)}{G_\ell} \tag{12}$$

4. LORENTZ GAS SOLUTION

If electron-electron collisions can be neglected in comparison with the electron-ion collisions, as is the case for large values of the plasma ionic charge, then an analytic solution of eq(3) can be obtained;

$$a_1 = -\frac{6D}{v_e^3 \nu_o Z} (x^2-x_o^2)^{\ell-1} x_o x \{x_o^2+\ell-x^2+[x^2-(2\ell+1)x_o^2]Sx_o^{-1}\}\{H(x-\alpha_-)-H(x-\alpha_+)\} \tag{13}$$

The current drive efficiency is given by

$$\frac{J}{P_d} = -\frac{2}{G_1 Z} \int_{\alpha_-}^{\alpha_+} x_o x^4 (x^2-x_o^2)^{\ell-1} \{x_o^2+\ell-x^2+[x^2-(2\ell+1)x_o^2]Sx_o^{-1}\} e^{-x^2} dx \tag{14}$$

For ℓ=1 this becomes

$$\frac{J}{P_d} = -\frac{2}{G_1 Z} [AJ_4 + BJ_6 + CJ_8 + S^3 J_{10}] \tag{15}$$

where $J_n = \int_{\alpha_-}^{\alpha_+} x^n e^{-x^2} dx$, (16)

$$A = u_o^3 + u_o - 3Su_o^2 , \tag{17}$$

$$B = 3u_o^2 S - u_o + 2S - 6u_o S^2 \tag{18}$$

$$C = S(3u_o S - 1 - 3S^2) \tag{19}$$

and G_1 is given by eq(A2) in the appendix. Values of J/P_d derived from eq(15) and multiplied by the factor $Z(Z+5)^{-1}$ (see Section 5) are plotted as a function of S for various values of u_o in Fig. 2. The current drive efficiencies obtained from the numerical solution of the full equation are also shown for comparison.

5. NUMERICAL SOLUTION

Equation (3) has been solved numerically using the two point boundary value code described by Cordey et al [6]. The discontinuities in R(x) at x =

α_- and $x = \alpha_+$ were smoothed as described in ref 6. Values of J/P_d were obtained for values $-3<u_o<3$, $0<S<2$, $Z = 1,2$ and harmonic numbers $\ell=1$ and $\ell=2$. Efficiencies for the fundamental frequency are listed in Table 1. More extensive tables for both X-mode and O-mode and for $\ell=1$ and $\ell=2$ are given in ref 7. Curves of J/P_d for the fundamental frequency are plotted against S in Fig. 2 for $u_o = 0.1$, 0.5, 1 and 3 respectively. As S increases from zero, the efficiency on the low field side increases dramatically whereas that on the high field side is reduced. For sufficiently large values of S the current on the high field side reverses although this occurs more readily for the lower values of u_o. This reversal takes place because the relativistic mass increase takes the gyrofrequency from above to below the wave frequency.

The dashed curves show the Lorentz gas results multiplied by the factor $Z(Z+5)^{-1}$ which relates the results of the full numerical calculation to the Lorentz values for $u_o>3$ in the non-relativistic case[1]. According to Cairns et al [4] this ratio should be maintained in the mildly relativistic case. This is indeed correct as is shown in Fig. 2 by the steadily improving agreement between the two calculations as u_o is increased. For $u_o=3$ the agreement is essentially complete, at least for values of S up to 0.5. However there are large differences between the numerical and renormalised Lorentz results, in both the relativistic and non-relativistic cases, for velocities $u_o< 1$ which are likely to be appropriate to near term experiments. The present non-relativistic numerical results agree well with those of Karney and Fisch[8] when these authors model the complete electron-electron collison operator through the use of a displaced Maxwellian background electron distribution.

In Fig.3 the efficiency, current and absorbed power for the $\ell=2$ case are plotted as a function of u_o for S = 0.06 and S = 0.24 and show the asymmetry about $u_o=0(\omega=\ell\Omega)$ which develops as the relativistic effects become significant.

6 RAY TRACING CALCULATIONS

In order to predict the effect of the relativistic resonance condition in a tokamak experiment, the results of the Fokker-Planck calculation have been incorporated into a ray tracing code. Ray tracing using the cold plasma dispersion relation has been discussed by, for example, Fidone et al[3] and Ott et al[9]. The present code uses the weakly relativistic expression for the dielectric tensor given by Shkarofsky[10] from which the absorption coefficient is obtained as described by Bornatici[11]. The power absorbed and the values of u_o and S were calculated at each point along the ray. The results obtained in the previous section for J/P_d were then used to obtain the current density profile.

Typical ray paths for X-mode, 60 GHz second harmonic electron cyclotron waves injected from the low field side into a tokamak of similar

size to DITE are shown in Fig 4. The major radius (R) was 1.17 m and the minor radius (a) was 0.26m. Plasma temperature and density profiles were taken to be parabolic in form, $T_e(r) = T_{eo}[1-(r/a)^2]$ and $n_e(r) = n_{eo}[1-(r/a)^2]$ with central values T_{eo} = 1keV and $n_{eo} = 10^{13}cm^{-3}$. The resonance surface $2\Omega = \omega$ passed through the magnetic axis and the rays were injected on the mid-plane at different angles ψ $(\simeq \tan^{-1}(k_{\parallel}/k_r))$ to the major radius. The total current obtained as a function of ψ is shown in Fig.5 for both the relativistic and non-relativistic calculations. In both cases more than 95% of the input power was absorbed for $\psi < 30°$. The major difference in the two curves appears at low values of ψ (small $k_{\parallel}$, large S) where the rapid drop in current predicted by the relativistic theory contrasts with the almost constant current given by the non-relativistic calculation. For these small values of $k_{\parallel}$ the Doppler shift component in the resonance condition plays only a minor role compared with the mass increase. Resonance is then determined largely by the energy, rather than the parallel velocity, of an electron and the current drive efficiency correspondingly falls. The discontinuity in current occurring at $\psi = 35°$ corresponds to the transition from a ray hitting the inside wall (case A) to one making a double pass through the resonance region (case B). For large angles the rays are unable to reach this region (case C). In addition the relativistic cut-off on the low field side operates to reduce the current generated by such rays.

From Fig.5 it can be seen that to sustain a plasma current of 100 kA would require 1.5 MW of ECRH power. On the basis of a calculation akin to that of Fielding[12] we find that, for this amount of power, the quasi-linear diffusion coefficient is still substantially less than that due to collisions so that our perturbation treatment remains valid.

In higher temperature tokamaks the relativistic effects will not be restricted to quasi-perpendicular propagation. For example, in the non-relativistic calculations of Edlington et al[13], for X-mode fundamental waves injected from the high field side into a JET-sized tokamak, a typical value of S is 0.2 for T_{eo}=10 keV and $N_{\parallel}$=0.6($N_{\parallel}=k_{\parallel}c/\omega$). The effective value of u_o was approximately three and so from Fig.2 one might expect a 30% reduction in the predicted current drive efficiency if the relativistic resonance condition were to be incorporated into these calculations.

7 SUMMARY

A full Fokker-Planck treatment of current drive by ECRH has been carried out with relativistic corrections applied to the resonance condition. The results are expressed in terms of u_o, which is the parallel velocity (normalised to v_e) of the resonant electrons in the non-relativistic case, and S which parameterises the relativistic effect. In this form the results can be readily incorporated into ray tracing codes. For $u_o > 3$ the values of J/P_d were found to be in good agreement with those obtained from a Lorentz gas model (electron-electron collisions neglected)

when the latter were multiplied by $Z(Z+5)^{-1}$ as suggested by Cairns et al [4]. However, for smaller values of u_o the renormalised Lorentz gas model substantially underestimates the current drive efficiency for almost all values of S. Ray tracing calculations for the example of second harmonic X-mode radiation strongly absorbed in a tokamak similar to DITE show a reduction in current drive efficiency as relativistic effects become important. This is expected to be a feature of all ECRH current drive schemes since it is due to the resonance condition becoming dominated by the energy dependent mass increase rather than the parallel velocity dependent Doppler shift.

Acknowledgements

We wish to thank J A Owen for the use of his code to calculate the relativistic dielectric tensor used in the ray tracing calculations.

REFERENCES

1 N J Fisch and A H Boozer, Phys Rev Lett, 45 (1980) 720.
2 I Fidone, G Granata and R L Meyer, Plasma Physics 22 (1980) 261
3 I Fidone, G Granata and R L Meyer, Phys.Fluids 25 (1982) 2249
4 R A Cairns, J Owen and C N Lashmore-Davies to be published in Phys. Fluids.
5 J G Cordey, T Edlington and D F H Start, Plasma Physics 24 (1982) 73.
6 J G Cordey et al, Nuclear Fusion 19 (1979) 249
7 D F H Start, M R O'Brien and P M V Grace, Culham Laboratory report CLM-R240 (1983).
8 C F F Karney and N J Fisch, Nuclear Fusion 21 (1981) 1549.
9 E Ott, B Hui and K R Chu, Phys.Fluids 23 (1980) 1031
10 I P Shkarofsky, Phys Fluids, 9(1966) 561
11 M Bornatici, Proc of Joint Workshop on Electron Cyclotron Emission Electron Cyclotron Resonance Heating, Oxford, July 1980, Culham Laboratory Report (CLM-EMR(1980)).
12 P J Fielding, Proc. Joint Workshop on Electron Cyclotron Emission and Electron Cyclotron Resonance Heating, Oxford, July 1980, Culham Laboratory Report (CLM-EMR(1980)).
13 T Edlington, J G Cordey, M O'Brien and D F H Start, Proc. 3rd Joint Varenna-Grenoble Int. Symp on Heating in Toroidal Plasmas 3 869, Grenoble 1982.

APPENDIX

The expression for the power density, eq(10), contains the integral G_ℓ defined by

$$G_\ell = \int_{\alpha_-}^{\alpha_+} x^3 (x^2-x_o^2)^{\ell-1}\left[x^2-x_o^2-\ell+2\ell x_o S\right]e^{-x^2}dx \qquad (A1)$$

Evaluating this integral for $\ell=1$ gives

$$G_1 = \frac{1}{2}\left[-S^2K_3+(1-2u_oS+2S^2)K_2 - (1+u_o^2-2u_oS)K_1\right] \qquad (A2)$$

where $K_n = \int_a^b y^n e^{-y}dy$, $a=\alpha_-^2$ and $b = \alpha_+^2$

The integrals K_n can be obtained from the recurrence relation:

$$K_n = nK_{n-1} + a^n e^{-a} - b^n e^{-b} \qquad (A3)$$

Similarly for $\ell=2$ we find

$$\begin{aligned} G_2 = \frac{1}{2}\Big[& S^4K_5-2S^2(1-2u_oS+2S^2)K_4 \\ & + (1-4u_oS+6S^2+6u_o^2S^2-12u_oS^3)K_3 \\ & - 2(1+u_o^2-4u_oS-2u_o^3S+6u_o^2S^2)K_2 \\ & + u_o^2(2+u_o^2-4u_oS)K_1\Big] \end{aligned} \qquad (A4)$$

TABLE 1 VALUES OF J/P_d FOR $\ell=1$ and $Z=1$

S	$U_o = -2.0$	-1.0	-0.5	-0.1	0.1	0.5	1.0	2.0
0.0	-2.87	-1.45	-0.82	-0.18	0.18	0.82	1.45	2.87
0.02	-2.68	-1.37	-0.76	-0.12	0.24	0.89	1.54	3.09
0.04	-2.51	-1.29	-0.69	-0.06	0.30	0.96	1.62	3.36
0.08	-2.22	-1.14	-0.56	0.06	0.43	1.09	1.79	4.17
0.12	-1.98	-1.00	-0.43	0.18	0.55	1.22	1.98	6.66
0.16	-1.76	-0.86	-0.31	0.30	0.66	1.35	2.18	0.00
0.20	-1.57	-0.73	-0.19	0.41	0.78	1.48	2.41	0.00
0.24	-1.39	-0.60	-0.08	0.52	0.88	1.59	2.66	0.00
0.3	-1.15	-0.43	0.08	0.66	1.02	1.73	0.00	0.00
0.6	-0.34	0.15	0.51	0.98	1.31	0.00	0.00	0.00
1.0	0.05	0.34	0.60	1.03	1.42	0.00	0.00	0.00
1.5	0.16	0.37	0.60	1.01	1.43	0.00	0.00	0.00
2.0	0.20	0.37	0.57	0.95	1.32	0.00	0.00	0.00

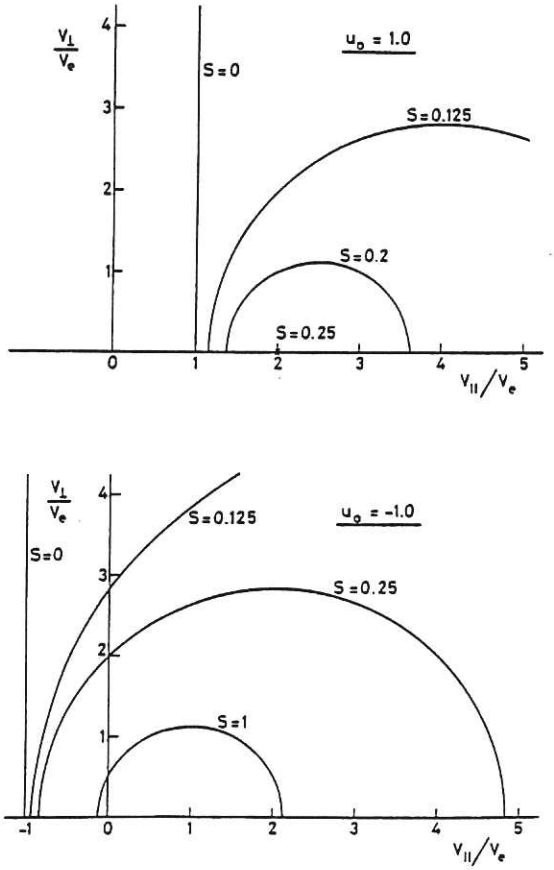

Fig.1 Electron-cyclotron resonance lines in velocity space for $u_o = 1$ and $u_o = -1$ for several values of S which parameterises the relativistic effect. Note the cut-off for $u_o = 1$ as S reaches the value 0.25.

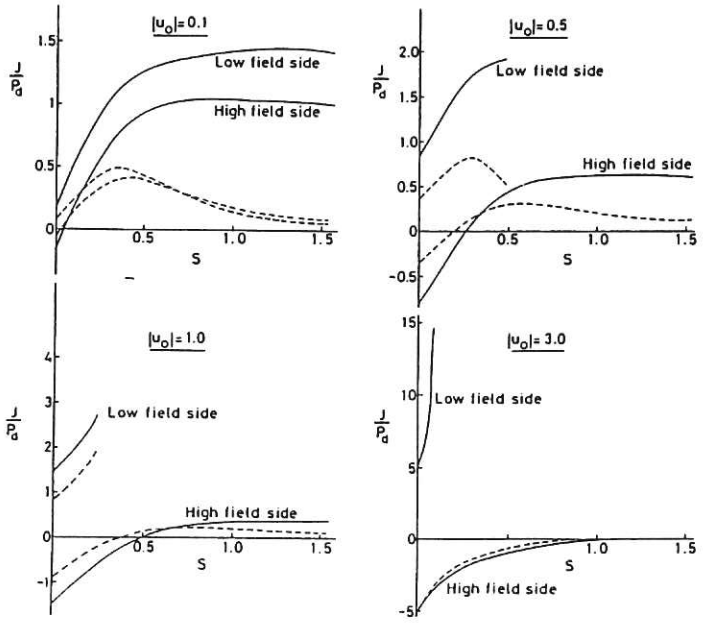

Fig.2 Current drive efficiency J/P_d versus S for $\ell = 1$ and $|u_o| = 0.1$, 0.5, 1 and 3. The curves labelled high (low) field side correspond to negative (positive) values of u_o. The cut-off on the low field side occurs for $S = (4u_o)^{-1}$. The dashed curves are the values obtained from the Lorentz gas model multiplied by $Z(Z + 5)^{-1}$.

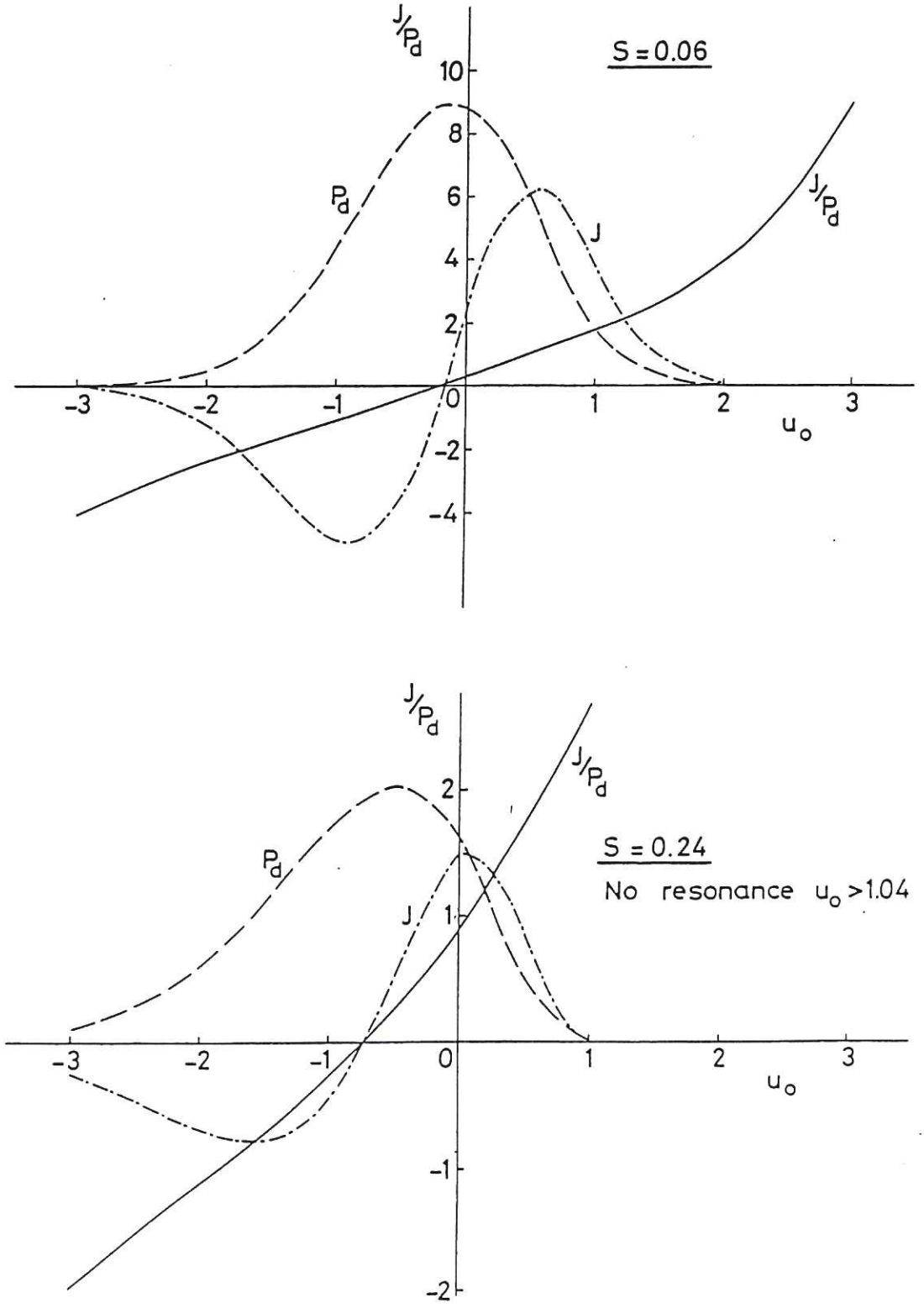

Fig.3 Curves of J/P_d, J and P_d versus u_o for $\ell = 2$ showing the loss of antisymmetry in the profiles as the value of S increases and relativistic effects become important. The power and current densities are expressed in arbitrary units. The cut-off on the low field side (positive u_o) occurs for $S = (4u_o)^{-1}$.

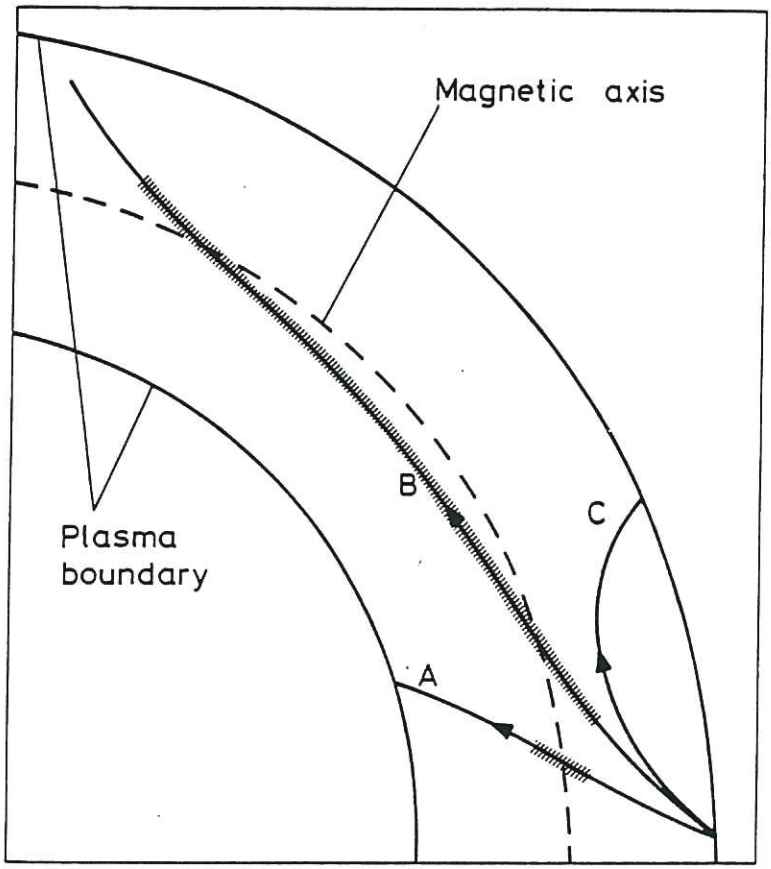

Fig.4 Plan view of ray paths for X-mode second harmonic cyclotron waves injected from the low field side into a tokamak with dimensions and plasma parameters similar to those of DITE. The rays A,B and C all originate in the median plane but at different angles ψ to the major radius.

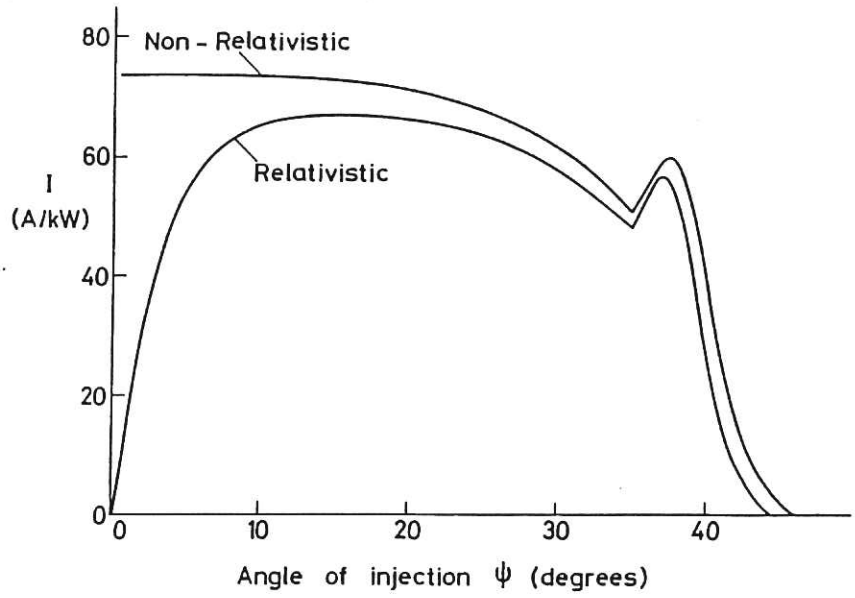

Fig.5 The current produced by rays such as those in Fig.4 versus the angle of injection to the major radius. Note the sharp reduction in current predicted by the relativistic calculation as the angle, and $k_{\parallel}$ become small.